NASA TECHNICAL NOTE

NASA TN D-6090

MEASURED AND CALCULATED VIBRATION PROPERTIES OF RING-STIFFENED HONEYCOMB CYLINDERS

by James A. Schoenster

Langley Research Center
Hampton, Va. 23365

NATIONAL AERONAUTICS AND SPACE ADMINISTRATION • WASHINGTON, D. C. • JANUARY 1971

1. Report No.	2. Government Accession No.	3. Recipient's Catalog No.
NASA TN D-6090		

4. Title and Subtitle

MEASURED AND CALCULATED VIBRATION PROPERTIES OF RING-STIFFENED HONEYCOMB CYLINDERS

5. Report Date: January 1971

6. Performing Organization Code:

7. Author(s)

James A. Schoenster

8. Performing Organization Report No.: L-7226

9. Performing Organization Name and Address

NASA Langley Research Center
Hampton, Va. 23365

10. Work Unit No.: 124-08-14-08

11. Contract or Grant No.:

12. Sponsoring Agency Name and Address

National Aeronautics and Space Administration
Washington, D.C. 20546

13. Type of Report and Period Covered: Technical Note

14. Sponsoring Agency Code:

15. Supplementary Notes

16. Abstract

This report describes an experimental and analytical investigation of the dynamic response characteristics of axisymmetric-ring-stiffened bonded-aluminum honeycomb cylinders. Good agreement between experiment and a finite-element analytical technique was obtained for both frequencies and mode shapes. Investigations into the variation of selected parameters, such as cylinder-edge restraint and bending stiffness of the end rings, showed that significant differences were obtained either in frequency while the associated mode shape was only slightly affected or in mode shape while the associated frequency was only slightly affected. Damping values were in the range of those reported for other honeycomb structures.

17. Key Words (Suggested by Author(s))	18. Distribution Statement
Ring-stiffened honeycomb cylinders Vibration properties	Unclassified – Unlimited

19. Security Classif. (of this report)	20. Security Classif. (of this page)	21. No. of Pages	22. Price*
Unclassified	Unclassified	51	$3.00

*For sale by the National Technical Information Service, Springfield, Virginia 22151

MEASURED AND CALCULATED VIBRATION PROPERTIES OF RING-STIFFENED HONEYCOMB CYLINDERS

By James A. Schoenster
Langley Research Center

SUMMARY

This report describes an experimental and analytical investigation of the dynamic response characteristics of axisymmetric-ring-stiffened bonded-aluminum honeycomb cylinders. Calculated natural frequencies and mode shapes were compared with experimental resonant frequencies and normalized resonant response shapes in order to evaluate a finite-element analytical representation of the cylinders. Even though some complicated mode shapes were caused by the rings, good to excellent agreement was obtained between the analysis and the experiment for unrestrained-edge conditions. Representation of a bolted joint by a clamped edge and of a hinged joint by a simply supported edge gave poor agreement in the comparison for some lower frequencies but gave good agreement in the comparison for mode shapes. Some of the discrepancies were attributed to the longitudinal restraint representation (implicit in the clamped and simply supported edges) assumed for the bolted and hinged joints. An analytical investigation into the effect of the bending stiffness of the end rings of the cylinder revealed an insensitivity of the natural frequency to this parameter; however, some of the mode shapes were considerably affected. Damping values were in the range of those reported for other honeycomb structures.

INTRODUCTION

Bonded honeycomb sandwich construction is used extensively in the aerospace industry in the design of many types of lightweight load-carrying structures. Shell sections such as launch-vehicle nose cones and shrouds are particularly adaptable to honeycomb design. Because of the interest in this efficient type of construction, many studies have been made into the dynamics of composite, sandwich, and stiffened shell-type structures, as indicated by a recent survey (ref. 1). Some examples of these studies include a free-vibration investigation of cylindrical shells with isotropic facings (ref. 2), a study of the effects of reduced-pressure environment on the vibration of flat sandwich panels (ref. 3), a study of sandwich beams (ref. 4), and an investigation of damping properties of sandwich beams (ref. 5). However, in all the studies into the dynamic behavior of the

shells, there is a paucity of experimental mode-shape data and of comparisons with analysis.

A recent effort to correlate analytical results and experimental data is reported in reference 6, in which both frequencies and nodal points of a honeycomb structure were used as bases for comparison. An analytical technique was developed in reference 6 for predicting the modes and frequencies of axisymmetric-ring-stiffened shells by using a thin-shell representation outlined in references 7 and 8. However, complete experimental mode-shape data and comparisons of available data with predicted results were not presented.

The purpose of the present paper is to report the results of a study to determine both mode shapes and frequencies of axisymmetric-ring-stiffened bonded-aluminum honeycomb cylinders. The experimental results are compared with values predicted by using the analytical techniques described in references 6 and 7. The significance of the end-ring bending stiffness (used in predicting the dynamic characteristics of the axisymmetric-ring-stiffened cylinders) is also considered. The model investigated is a scaled version of a potential shroud section for a Saturn V launch-vehicle payload. It consists of two cylinder sections which can be joined together by means of standard fasteners, representing a typical end attachment, and which are used individually and in combination to form three configurations. Three different edge conditions were investigated, and the analytical representations of these restraints are discussed. Damping values were experimentally determined for several modes of the cylinder.

SYMBOLS

a	distance from axis of shell to origin of ξ_1,ξ_3 axes, cm
C_{11},C_{12},C_{22}	membrane stiffness parameters, N/m
C_{66}	shear stiffness of shell, N/m
D_{11},D_{12},D_{22}	flexural stiffness parameters, N-m
D_{66}	torsional stiffness of shell, N-m
d	diameter of test cylinder, cm
E	modulus of elasticity, N/m^2

EA	extensional stiffness of ring, MN
EI_1	bending stiffness of ring about ξ_1-axis, N-m^2
EI_3	bending stiffness of ring about ξ_3-axis, N-m^2
EI_{13}	bending stiffness of ring due to coupling between bending about ξ_1-axis and bending about ξ_3-axis, N-m^2
f_n	resonant frequency, Hz
Δf	change in frequency, Hz
GJ	torsional rigidity of ring, N-m^2
h_c	half the core thickness of honeycomb (fig. 2), cm
h_f	face-sheet thickness (fig. 2), cm
$K_{11},K_{12},K_{22},K_{66}$	stiffness parameters representing interaction between in-plane and out-of-plane strains, N
l	length of test cylinder, cm
M	mass per unit surface area, kg/m^2
m_1	mass of ring per unit circumferential length, kg/m
m_2	mass moment of inertia of ring cross section about ξ_3-axis, mg-cm
m_3	mass moment of inertia of ring cross section about ξ_1-axis, mg-cm
n	number of circumferential waves
s	meridional coordinate (fig. 5), cm
u,v,w	components of middle surface displacements in meridional, circumferential, and normal directions, respectively

ϵ_n	element length (n = 1, 2, . . . 7), cm
$\Delta\theta$	change in phase angle, radians
μ	damping factor equal to twice the ratio of structural damping to critical damping for an equivalent viscous damped system
ν	Poisson's ratio
ξ_1, ξ_3	coordinates which locate a point in ring cross section (fig. 5), cm
$\hat{\xi}_1, \hat{\xi}_3$	coordinates of point of attachment of ring to shell, cm
ϕ	angle between normal to shell axis and normal to shell surface at ring attachment circumference, deg

Subscript:

max	maximum

APPARATUS AND TEST CONDITIONS

Description of Models

The test models are designated cylinder 1, cylinder 2, and cylinder 3, and their physical parameters are given in table I. Cylinders 1 and 2 have diameters of 66.04 cm; cylinder 1 is 16.22 cm long and cylinder 2 is 60.45 cm long (figs. 1(a) and 1(b)). These two cylinders were combined by means of 54 nut and bolt fasteners to obtain cylinder 3, which is 76.67 cm long (fig. 1(c)). Each of the basic sections has a core of 0.00254-cm-thick 3003-H19 aluminum alloy forming a 0.18726-cm cell size to which 0.00508-cm-thick face sheets of 5052-H19 aluminum alloy were bonded by using a combination of an epoxy resin and a copolymer.

At the top and bottom of cylinders 1 and 2 are rings which provide a method for connecting the cylinders to adjoining cylindrical sections by means of a butt joint which uses 54 nut and bolt fasteners. The machined 6061-T6 aluminum-alloy end rings are designated as ring 1 and ring 4, with details as shown in figure 2. At ring 4 of cylinders 1 and 2, the joint is made to form cylinder 3. Torsional stiffness was added to these rings by means of 54 equally spaced clips of cast aluminum (see fig. 1). Cylinder 2 has two additional internal rings (rings 2 and 3), the details of which are shown in figure 2. The

outside face sheets are continuous across these internal rings, and the resulting total shell thickness for each section is 0.3175 cm (see fig. 2).

The density of the individual honeycomb sections was determined by weighing each of the sections and subtracting the experimentally determined weight of the rings from the total weight. Differences in M (see table I) were attributed to the amount of bonding agent used to form the honeycomb sections.

Test Conditions

The tests conducted on the models are summarized in table II. The term "unrestrained" is used to describe the test condition for which the model is supported by four long strings, with rubber bands at the ends, spaced 90° apart. The term "standard fasteners" or "bolted joint" is used to describe the condition for which 54 nut and bolt fasteners attach ring 4 to a test stand. The mating ring of the test stand weighs 45 times the weight of the entire model; thus any dynamic interaction between the stand and the shell is avoided. The term "hinged joint" describes the condition for which 54 individual hinges are attached at each of the 54 bolt attachment locations and then, in turn, are connected to the test stand.

Tests, for the unrestrained condition, were also conducted on rings 1 and 4 completely separated from the shells; the clips, however, were still attached.

Instrumentation

A schematic view of the instrumentation used for the tests is given in figure 3. Relative amplitudes were measured with a noncontacting displacement measuring system. This system uses a servocontrolled noncontacting displacement probe mounted on a trolley and allows the investigator to continuously reconstruct a model mode shape on an x-y plotter without affecting the cylinder response in any manner. This system is similar to that described in reference 9.

Input force and acceleration were measured by means of small crystal transducers, and tests conducted on the cylinders indicated that this additional mass had a negligible effect on the resonant frequencies or mode shapes of the configurations tested.

Complex plane plots, which were used to determine damping, were obtained by using a commercially available vector-component-resolver tracking filter system and were recorded on an $x\text{-}y_1y_2$ plotter.

EXPERIMENTAL PROCEDURE

The dynamic response of the cylinders was determined by connecting an electromagnetic shaker (fig. 1(c)) to the structure and vibrating the model at a constant sinusoidal force input while increasing the frequency at a slow sweep rate. Frequencies at which both the amplitude was a maximum and the phase angle between the input force and acceleration was approximately 90° were defined as resonant frequencies, and it was at these frequencies that mode shapes were measured. In order to avoid nodal points for some of the modes, it was necessary to vary the location of the shaker attachment; thus, the shaker was attached to the model at various positions along a generator on the cylinder. All the modes presented in this report were obtained when the shaker was connected on this generator at one of the stiffening rings.

Damping was obtained by using the phase-change method described by Mead (ref. 10). By this method the damping factor μ (twice the ratio of structural damping to critical damping for an equivalent viscous damped system) is calculated from

$$\mu = \frac{2}{f_n \frac{\Delta\theta}{\Delta f}} \tag{1}$$

where $\Delta\theta/\Delta f$ is the change of the phase angle in radians with respect to the change of frequency in hertz at the resonant frequency. The method used in this report to determine f_n and $\Delta\theta/\Delta f$ is the Kennedy-Pancu complex plane plot (ref. 11). An example of this method of data interpretation is shown in figure 4. The quadrature component of acceleration is plotted as a function of the in-phase and out-of-phase components of acceleration referenced to force. Below this plot is a curve showing frequency as a function of the in-phase and out-of-phase components, which are used to correlate the two curves. A "best circle" is fitted to the complex-plane-plot data, and a diameter parallel to the quadrature axis, locates the resonant frequency f_n at one intersection with the circle and the "displaced origin" at the other intersection. A small change in phase angle $\Delta\theta$ is selected on the "resonant peak," and the resulting change in frequency Δf is then determined. In this example, the resulting damping factor μ is equal to 0.005. Additional examples of this approach may be found in reference 12.

ANALYTICAL PROCEDURE

Method

This analytical procedure used in this investigation is described in references 6, 7, and 8. The alternate procedure for joining rings to shells in reference 6 is the method

used in the present study. In general, the procedure is based on axisymmetric line connections between the ring and shell. The shell is represented by finite elements, as described in reference 7, and the equations are developed by using thin-shell theory. It was assumed in the present study that the honeycomb works only as an ideal spacer for the face sheets and offers no stiffness to the shell. The equations used to calculate the required stiffnesses of the shell are as follows:

$$C_{11} = C_{22} = \frac{2Eh_f}{1 - \nu^2} \tag{2}$$

$$C_{12} = \nu C_{11} \tag{3}$$

$$C_{66} = \frac{1 - \nu}{2} C_{11} \tag{4}$$

$$D_{11} = D_{22} = \frac{2E\left[(h_f + h_c)^3 - h_c^3\right]}{3(1 - \nu^2)} \tag{5}$$

$$D_{12} = \nu D_{11} \tag{6}$$

$$D_{66} = 2D_{11}(1 - \nu) \tag{7}$$

$$K_{11} = K_{12} = K_{22} = K_{66} = 0 \tag{8}$$

The rings are idealized by the direct-stiffness method. Complete details of the program used to compute the results may be found in reference 8.

Analytical Representation of the Models

Shown in figure 5 and table I is the analytical representation of the models. Figure 5 shows the shell wall and the attachment locations of the rings to the wall. The rings are attached at element junctures, shown as dashed lines, and are connected to the middle surface of the shell. The clips used on rings 1, 4, and 5 add to the ring mass and are not considered to have other effects in the analysis. Specific details for each of the cylinders are given in the following paragraphs.

Cylinder 1 (fig. 5(a)) is represented by a honeycomb shell section 13.44 cm long, having five elements whose lengths are given in table I(b). Rings 1 and 4 are attached at

the ends of the shell, which for the five-element representation are junctures 1 and 6, respectively.

Cylinder 2 (fig. 5(b)) is represented by a continuous honeycomb shell section 57.66 cm long, having seven elements whose lengths are given in table I(b). Rings 1 and 4 are attached at the ends of the shell, which for a seven-element representation are junctures 1 and 8, respectively. Rings 2 and 3 are attached to the shell at junctures 3 and 6, respectively.

Cylinder 3 (fig. 5(c)) is represented by a continuous honeycomb shell section 73.88 cm long, having six elements whose lengths are given in table I(b). Ring 1 is attached at both ends of the shell, which for a six-element representation are junctures 1 and 7. Rings 2 and 3 are attached to the shell at junctures 2 and 5, respectively. Ring 5, which consists of two rings back to back, is attached at juncture 6.

Representation of Edge Conditions

The analytical representation of the string support is a free edge. The analytical representation of the standard fasteners to the test stand is a clamped edge. The analytical representation of the hinged connection to the test stand is a simply supported edge. A complete description of these edge conditions may be found in reference 7. In general, the clamped edge restrains motion in the u, v, and w directions and also restrains rotation of the shell generator relative to the unstrained direction. The simply supported edge restrains motion in the u, v, and w directions but places no restriction on rotations.

Parameters

Two parameters were selected for a computer study to assist in evaluating their significance in the prediction of the modes and frequencies of the models. The selected parameters are the longitudinal restraint at the edge and the bending stiffness of the end rings EI_1. These two parameters are very difficult to determine in actual aerospace construction. The amount of end restraint provided by nut and bolt fasteners is not completely understood, and a clamped edge may not be the best representation. The end rings of these cylinders represent the joints used to connect sections together and, in many cases, these joints have extremely complicated design details because of local strength requirements. These details make the calculation of the bending stiffness difficult.

The variations on these parameters were arbitrarily selected and are as follows:

(1) Relaxing the restraint on the deflection u of cylinder 2 with clamped edges.

(2) Increasing by 50 percent the bending stiffness EI_1 of rings 1 and 4 for cylinder 2 with free edges.

(3) Increasing by 50 percent the bending stiffness EI_1 of ring 4 and decreasing by 50 percent the bending stiffness EI_1 of ring 1 for cylinder 2 with free edges.

RESULTS AND DISCUSSION

The results of this study are presented in figures 6 to 19. The modes and frequencies of the three cylinders with the various edge restraints are presented first. Figures 6 to 10 show the comparisons of experiment and calculation in terms of frequency as a function of the number of circumferential waves n. Curves are faired through the data points to indicate trends, but no physical significance should be given to frequencies other than at integral values of n. Table III is a compilation of these frequencies. Figures 11 to 15 show the comparisons of experiment and calculation in terms of normalized mode shapes. The radial component of amplitude is plotted along a generator of the cylinder and is normalized to the maximum radial amplitude. The distance along the cylinder is measured from the top of ring 1. Also shown in these figures are the frequencies and circumferential wave numbers. Figure 16 shows a comparison of the calculated frequencies for the clamped-edge cylinder and the u-deflection-released cylinder in terms of the number of circumferential waves.

The effects of the ring properties are presented in figures 17 to 19. Figure 17 shows a comparison of experimental and calculated frequencies for various values of n for the end rings separated from the shells. Figure 18 shows the effect of varying the bending stiffness of the end rings in the calculations of frequency for several values of n and presents experimental frequencies for comparison. Figure 19 shows the effect of varying the bending stiffness on the predicted mode shapes.

Resonant frequencies determined by the Kennedy-Pancu method and damping factors obtained from the Kennedy-Pancu plots are presented in table IV.

Modes and Frequencies

Unrestrained-edge (free-edge) conditions.- The analysis gave good frequency results for the cylinders having free edges (see figs. 6, 7, and 8) over the range of modes investigated. Excellent agreement was obtained for the mode shapes of cylinders 2 and 3 in the range of n from 2 to 7 (see figs. 12 and 13). In general, the agreement between experimental and calculated mode shapes for cylinder 1 was good; however, for some of the modes, experimental data indicated a local bending at the end of this cylinder, whereas analysis did not predict this phenomenon (for example, see the mode at an experimental frequency value of 38.8 Hz in fig. 11). No explanation for this bending was

determined in the present study. Other deviations from the predicted mode shapes were observed, such as the wiggles at experimental values of 326.2 Hz in figure 11 and 159.6 Hz in figure 12; however, these wiggles were attributed to difficulties in the instrumentation and are not considered significant.

The radial components of amplitude along a generator for cylinders 2 and 3 (figs. 12 and 13) do not behave like those for cylinder 1 (fig. 11). For cylinder 1, the components of amplitude are all in phase at the lowest frequency mode for all values of n and they all have one nodal line near the center of the cylinder at the second lowest frequency mode for all values of n. These modes for cylinders 2 and 3 cannot be described in such a manner. For example, as shown in figure 12, the lowest frequency mode at $n = 5$ has a nodal line near one end of the cylinder. The lowest frequency mode for $n = 6$ has not only a nodal line near one end of the cylinder but considerable curvature at the opposite end. These complex mode shapes are attributed to complicated ring effects which make simple descriptions of the various mode shapes difficult.

Restrained-edge conditions.- Representing the standard fasteners as clamped edges and the hinged joints as simply supported edges did not result in as high a degree of analytical-experimental correlation as was achieved for the free-edge condition. For cylinder 2 the measured frequencies differed from the calculated frequencies by as much as 12.5 percent for modes with values of n from 4 to 8 (figs. 9 and 10). For the modes with $n = 2$ and $n = 3$, the difference was much greater, reaching almost 100 percent at $n = 2$ for cylinder 2 with hinged joints (fig. 10). The predicted and measured normalized mode shapes for cylinder 2 were in excellent agreement for all values of n (figs. 14 and 15).

Analysis indicated that there should be little difference (less than 1 percent) between the calculated frequencies for the clamped-edge cylinder and the simply supported cylinder (compare calculated frequency values in figs. 14 and 15). For cylinder 2 with standard fasteners, asymmetries in the cylinder caused two similar modes to occur at $n = 2$ and at $n = 3$. Experimentally, the largest difference between the frequency when standard fasteners were used and when hinged joints were used was approximately 18 percent for the $n = 2$ mode. However, for the modes above $n = 3$, there is less than a 2.6-percent difference in experimental frequencies for the two conditions.

The analytical investigation into the clamped-edge condition indicated that a releasing of the restraint on u at the clamped edge caused little change in the radial components of amplitudes; however, the predicted frequencies at $n = 2$ and $n = 3$ reduce to approximately one-eighth and one-half of their original values, respectively, as shown in figure 16. Since using just this variation of parameters caused the predicted

frequencies to bound the experimental frequencies by wide margins, far more understanding of these types of boundary restraint is needed to obtain a good mathematical representation.

Effects of Ring Properties

Properties of rings 1 and 4.- A study of rings 1 and 4 (with clips) was conducted to investigate the accuracy of their representation in the mathematical model. The natural frequencies of these rings were calculated by using the same mass and stiffness matrices that are used as input in the ring-stiffened-shell program. These frequencies are compared with experimentally obtained frequencies of the rings in both the in-plane direction and the out-of-plane direction, and a plot of frequency as a function of the number of circumferential waves is shown for rings 1 and 4 in figures 17(a) and 17(b), respectively. The in-plane modes for both rings show correlations of better than 5 percent, while the calculated frequencies in the out-of-plane direction are, at best, approximately 60 percent of the experimental frequencies. The differences between calculated and experimental out-of-plane frequencies were attributed to the inadequacies of the assumption that the clips add only mass.

Effect on cylinder response.- Although the out-of-plane frequencies of rings 1 and 4 were not accurately predicted from the mathematical model, there was good experimental-analytical correlation between both the mode shapes and frequencies for all the cylinders with free edges. This agreement indicates that the out-of-plane stiffnesses of rings 1 and 4 do not have much effect on the response of these cylinders. In addition, ring 5 in cylinder 3 is composed of two rings back to back and, as stated previously, the experimental-analytical correlations for this cylinder were excellent.

Further investigation into the effects of the end rings on the response of the cylinders was conducted analytically by varying the parameter EI_1 of rings 1 and 4. Shown in figure 18 is a comparison of the frequencies predicted by using three bending-stiffness conditions: (1) EI_1 calculated from the structure, (2) increasing EI_1 50 percent for rings 1 and 4, and (3) increasing EI_1 50 percent for ring 4 and decreasing EI_1 50 percent for ring 1.

A band covering ±11 percent of a mean value would encompass all three conditions for the lowest mode for any value of n; bands covering ±6 percent and ±7 percent would suffice for the second lowest mode and third lowest mode, respectively. These boundaries completely enclose all frequencies obtained, and if just the condition of EI_1 being increased by 50 percent for both rings were considered, the percentage deviation would be less than ±5 percent. It may also be noted that the curves all follow the same general

trend. Thus, in order to obtain good predictions of the resonant frequencies in the present investigation, it is not necessary to know very accurately the bending stiffness in either the in-plane or out-of-plane direction of the end rings.

While the parameter EI_1 does not have a major effect on the resonant frequencies of the free-edge cylinders, it does affect the mode shapes. Previously, it was shown that excellent experimental-analytical agreement was obtained for the mode shapes up to values of $n = 7$. With variations on EI, significant differences can be observed; for example, in figure 19(a) the lowest frequency mode that exhibits a node line occurs at $n = 3$ for the case of decreasing EI_1 of ring 1 and increasing EI_1 of ring 4, at $n = 5$ for the calculated EI_1, and at $n = 6$ for the case of increasing EI_1 of rings 1 and 4. Other gross discrepancies can be observed in the mode shapes, with the worst being for the second lowest mode at $n = 7$ (fig. 19(b)).

Structural Damping

Structural damping factors, equal to twice the ratio of structural damping to critical damping for an equivalent viscous damped system (see eq. (1)), and resonant frequencies determined from the Kennedy-Pancu plots for cylinder 2 supported on strings are presented in table IV. The resonant frequencies determined from the complex plane plots concurred with those determined by selecting peak amplitudes which had a phase angle between input force and acceleration of close to 90°. In addition, the complex plane plots indicated there was little off-resonant contribution to the various modes. The maximum difference between resonant frequencies obtained by the two methods was only 2.3 percent, which occurred for the fourth lowest frequency mode at $n = 5$.

Damping factors μ ranged from 0.016 for the second lowest frequency mode at $n = 2$ to 0.004 for both the second lowest frequency mode at $n = 5$ and the third lowest frequency mode at $n = 6$. With damping values this low, the differences in the predicted shapes and the resonant frequencies with and without damping would be negligible. Comparison of these damping values with equivalent damping values computed from experimental logarithmic decrements reported in reference 5 shows the damping to be slightly lower for the present cylinders, but not significantly so when considering the accuracy of damping measurements.

CONCLUDING REMARKS

An experimental and analytical investigation of the dynamic response characteristics of axisymmetric-ring-stiffened bonded-aluminum honeycomb cylinders has been

conducted. Calculated natural frequencies and mode shapes were compared with experimental resonant frequencies and normalized resonant response shapes in order to evaluate a finite-element analytical representation of the cylinders. Three configurations having length-diameter ratios of 0.25, 0.92, and 1.16 were investigated with free edges. In addition, the cylinder with a length-diameter ratio of 0.92 was studied with two types of edge restraints.

It was determined that both mode shapes and resonant frequencies can be adequately predicted for cylinders having free edges. Rings produced complicated mode shapes; however, the analysis predicted these mode shapes with excellent agreement for the cylinders having length-diameter ratios of 0.92 and 1.16. Some discrepancy in the mode shapes was observed at the end of the cylinder with a length-diameter ratio of 0.25, where the analysis did not predict a sharp change in curvature as was observed experimentally in some of the modes.

The agreement between predicted and experimental frequencies for the restrained-edge conditions was poor for the lower values of circumferential wave number n (values of 2, 3, and 4) but was better for the higher values of n. An analytical investigation into the representation of the edge restraint showed a significant sensitivity of the predicted frequencies to this parameter (variations of almost 100 percent for the lower values of n). The predicted and measured mode shapes were in excellent agreement for all values of n and were not significantly affected by the edge restraint.

In this study, it was determined that an accurate representation of neither the in-plane nor out-of-plane stiffness of the end rings was necessary to obtain good frequency predictions for the cylinders. In addition, good mode-shape agreement between calculations and experiment for the cylinders was obtained when using a poor representation of the out-of-plane stiffness of the end rings. However, significant differences were observed in the calculated and experimental mode shape of a cylinder when the in-plane stiffness of the end rings was varied in the analysis. The damping values of these honeycomb cylinders are in the range of those for other reported honeycomb structures.

Langley Research Center,
National Aeronautics and Space Administration,
Hampton, Va., October 1, 1970.

REFERENCES

1. Bert, Charles W.; Egle, Davis M.: Dynamics of Composite, Sandwich, and Stiffened Shell-Type Structures. J. Spacecraft Rockets, vol. 6, no. 12, Dec. 1969, pp. 1345-1361.

2. Yu, Yi-Yuan: Vibrations of Elastic Sandwich Cylindrical Shells. Trans. ASME, Ser. E: J. Appl. Mech., vol. 27, no. 4, Dec. 1960, pp. 653-662.

3. Powell, Clemans A., Jr.; and Stephens, David G.: Vibrational Characteristics of Sandwich Panels in a Reduced-Pressure Environment. NASA TN D-3549, 1966.

4. Clary, Robert R.; and Leadbetter, Sumner A.: An Analytical and Experimental Investigation of the Natural Frequencies of Uniform Rectangular-Cross-Section Free-Free Sandwich Beams. NASA TN D-1967, 1963.

5. Bert, C. W.; Wilkins, D. J., Jr.; and Crisman, W. C.: Damping in Sandwich Beams With Shear-Flexible Cores. Trans. ASME, Ser. B: J. Eng. Ind., vol. 89, no. 4, Nov. 1967, pp. 662-670.

6. Steeves, Earl C.; Durling, Barbara J.; and Walton, William C., Jr.: A Method for Computing the Response of a General Axisymmetric Shell With an Attached Asymmetric Structure. AIAA Structural Dynamics and Aeroelasticity Specialist Conference and the ASME/AIAA 10th Structures, Structural Dynamics, and Materials Conference, Apr. 1969, pp. 302-328.

7. Adelman, Howard M.; Catherines, Donnell S.; and Walton, William C., Jr.: A Method for Computation of Vibration Modes and Frequencies of Orthotropic Thin Shells of Revolution Having General Meridional Curvature. NASA TN D-4972, 1969.

8. Adelman, Howard M.; Catherines, Donnell S.; Steeves, Earl C.; and Walton, William C., Jr.: User's Manual for a Digital Computer Program for Computing the Vibration Characteristics of Ring-Stiffened Orthotropic Shells of Revolution. NASA TM X-2138, 1970.

9. Naumann, Eugene C.; and Flagge, Bruce: A Noncontacting Displacement Measuring Technique and Its Application to Current Vibration Testing. Preprint No. 16.18-5-66, Instrum. Soc. Amer., Oct. 1966.

10. Mead, D. J.: The Internal Damping Due to Structural Joints and Techniques for General Damping Measurement. C.P. No. 452, Brit. A.R.C., 1959.

11. Kennedy, Charles C.; and Pancu, C. D. P.: Use of Vectors in Vibration Measurement and Analysis. J. Aeron. Sci., vol. 14, no. 11, Nov. 1947, pp. 603-625.

12. Schoenster, James A.; and Clary, Robert R.: Experimental Investigation of the Longitudinal Vibration of a Representative Launch Vehicle With Simulated Propellants. NASA TN D-4502, 1968.

TABLE I.- MODEL DESCRIPTION

(a) Properties of cylinders 1, 2, and 3

Property	Cylinder 1	Cylinder 2	Cylinder 3
l, cm . . .	16.22	60.45	76.67
d, cm . . .	66.04	66.04	66.04
l/d	0.25	0.92	1.16

(b) Properties of shells for cylinders 1, 2, and 3

Property	Cylinder 1	Cylinder 2	Cylinder 3
M, kg/m^2 . . .	0.7329	0.6623	0.6623 0.7329
h_c, cm	0.15367	0.15367	0.15367
h_f, cm	0.00508	0.00508	0.00508
ν	0.33	0.33	0.33
ϵ_1, cm	2.54	6.22	12.57
ϵ_2, cm	2.54	6.35	10.92
ϵ_3, cm	2.54	10.92	10.16
ϵ_4, cm	2.54	10.16	10.19
ϵ_5, cm	3.28	10.19	15.21
ϵ_6, cm		7.60	14.83
ϵ_7, cm		6.22	

(c) Properties of rings

Property	Ring 1	Ring 2	Ring 3	Ring 4	Ring 5
$\hat{\xi}_1$, cm	*0.820	0	0	-0.818	0
$\hat{\xi}_3$, cm	-0.0393	0	0.0594	0.00137	0.00137
ϕ, deg	90	90	90	90	90
EI_1, N-m^2 . . .	4.355	0.3007	9.110	2.791	5.581
EI_3, N-m^2 . . .	29.90	4.811	4.813	24.58	213.9
EI_{13}, N-m^2 . . .	-2.695	0	0	-0.2797	0
EA, MN	1.297	2.864	3.242	1.229	2.458
GJ, N-m^2	0.08943	3.049	3.073	0.08443	0.1689
a, cm	32.900	32.861	32.802	32.847	32.847
m_1, kg/m	0.06978	0.1116	0.1263	0.06753	0.1350
m_2, mg-cm . . .	16.07	1.875	1.876	13.51	117.5
m_3, mg-cm . . .	2.342	0.1172	3.550	1.533	3.066

*Except for cylinder 3 at juncture 7, where $\hat{\xi}_1 = -0.820$.

TABLE II.- SUMMARY OF CONDITIONS USED FOR EXPERIMENTAL-ANALYTICAL COMPARISONS

Section	Edge restraints		
	Unrestrained (Free edge)	Standard fasteners (Clamped edge)	Hinged joint (Simply supported edge)
Cylinder 1	✓		
Cylinder 2	✓	✓	✓
Cylinder 3	✓		
Ring 1 (with clips)	✓		
Ring 4 (with clips)	✓		

TABLE III.- SUMMARY OF FREQUENCIES

(a) Cylinder 1; unrestrained edges

n	Frequency, Hz			
	Mode 1		Mode 2	
	Exp.	Calc.	Exp.	Calc.
2	25.8	25.1	38.8	32.2
3	71.8	70.8	109.8	96.2
4	136.4	134.9	196.3	177.9
5	220.4	216.8	300.4	276.8
6	326.2	316.1	422.7	394.6
7	----	432.9	561.2	531.8
8	564.4	566.9	----	----

(b) Cylinder 2; unrestrained edges

n	Frequency, Hz							
	Mode 1		Mode 2		Mode 3		Mode 4	
	Exp.	Calc.	Exp.	Calc.	Exp.	Calc.	Exp.	Calc.
2	24.6	23.5	31.1	29.3	----	----	----	----
3	69.7	65.6	84.7	79.6	----	----	----	----
4	131.7	123.7	159.6	148.9	414.9	413.8	----	----
5	208.6	193.9	255.2	236.8	379.9	374.1	563.0	537.1
6	291.2	268.6	363.4	341.3	440.1	423.8	569.7	533.6
7	378.6	344.5	488.4	460.7	538.2	526.6	----	----

(c) Cylinder 3; unrestrained edges

n	Frequency, Hz							
	Mode 1		Mode 2		Mode 3		Mode 4	
	Exp.	Calc.	Exp.	Calc.	Exp.	Calc.	Exp.	Calc.
2	24.7	23.6	28.6	27.6	----	----	----	----
3	70.3	65.8	79.4	76.1	382.9	380.5	----	----
4	133.9	124.2	150.1	143.7	300.6	292.1	521.0	526.1
5	212.1	194.9	239.5	230.0	327.3	311.2	----	456.4
6	291.3	269.7	345.7	333.5	417.8	396.6	497.2	478.0
7	378.6	345.0	447.4	452.2	536.4	516.1	----	----

TABLE III.- SUMMARY OF FREQUENCIES – Concluded

(d) Cylinder 2; restrained edge (standard fasteners)

n	Frequency, Hz					
	Mode 1		Mode 2		Mode 3	
	Exp.	Calc.	Exp.	Calc.	Exp.	Calc.
2	108.0 123.0	195.2	----	----	----	----
3	94.7 91.7	127.0	----	----	----	----
4	138.2	142.0	324.6	359.6	----	----
5	209.6	200.3	340.2	355.2	519.8	517.5
6	291.4	270.9	420.8	420.0	550.2	526.3
7	379.3	345.0	----	----	----	----
8	477.6	425.5	----	----	----	----

(e) Cylinder 2; restrained edge (hinged joint)

n	Frequency, Hz			
	Mode 1		Mode 2	
	Exp.	Calc.	Exp.	Calc.
2	102.6	194.2	----	----
3	84.8	126.5	----	----
4	135.6	141.7	316.4	356.2
5	208.2	200.2	337.0	352.6
6	289.9	270.8	416.7	418.4
7	379.6	345.0	----	----
8	478.8	425.5	----	----

TABLE IV.- RESONANT FREQUENCIES AND DAMPING FACTORS
OBTAINED FROM KENNEDY-PANCU PLOTS FOR
CYLINDER 2 WITH STRING SUPPORT

n	Mode 1		Mode 2		Mode 3		Mode 4	
	Frequency, Hz	Damping factor μ	Frequency, Hz	Damping factor μ	Frequency, Hz	Damping factor μ	Frequency, Hz	Damping factor μ
2	24.6	0.008	30.9	0.016	----	----	----	----
3	69.1	.008	83.7	.005	----	----	----	----
4	131.0	.015	157.9	.005	410.6	0.007	----	----
5	207.1	.006	253.0	.004	379.8	.005	550.6	0.007
6	289.7	.007	360.3	.005	437.6	.004	567.5	.005
7	377.8	.005	482.9	.005	536.7	.005	----	----

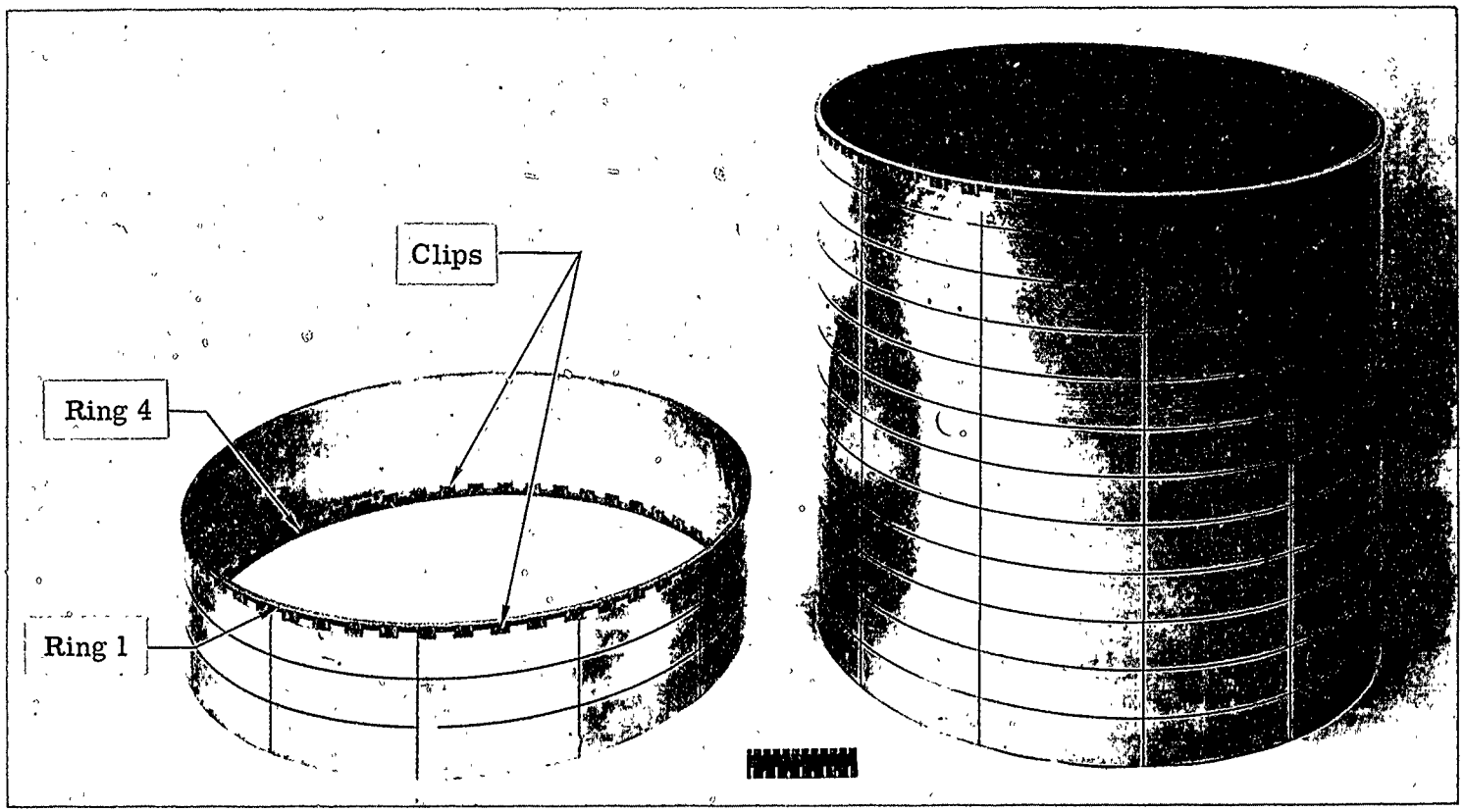

(a) Cylinder 1. (b) Cylinder 2.

Figure 1.- The honeycomb cylinders.

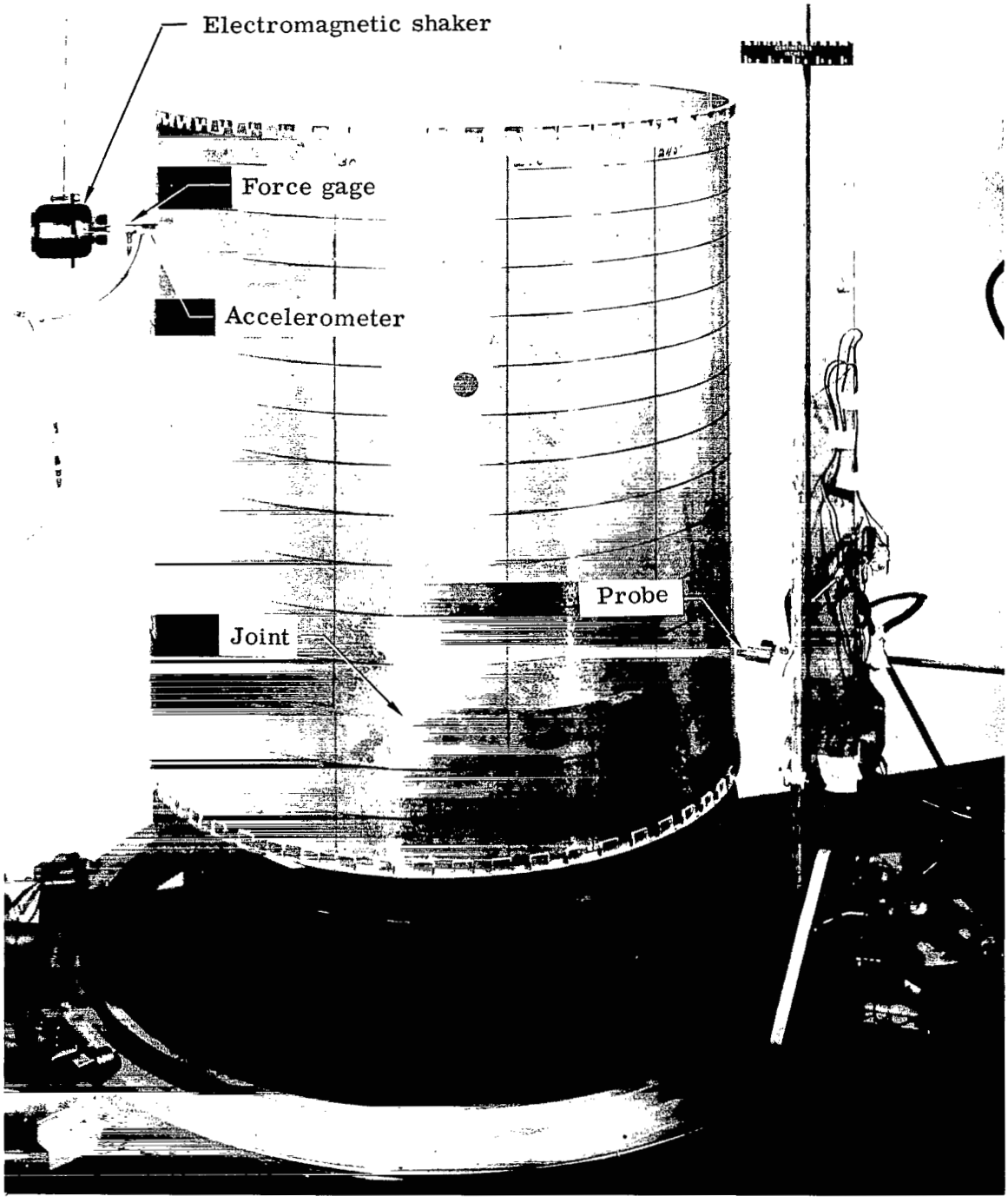

(c) Cylinder 3. L-70-3322.1

Figure 1.- Concluded.

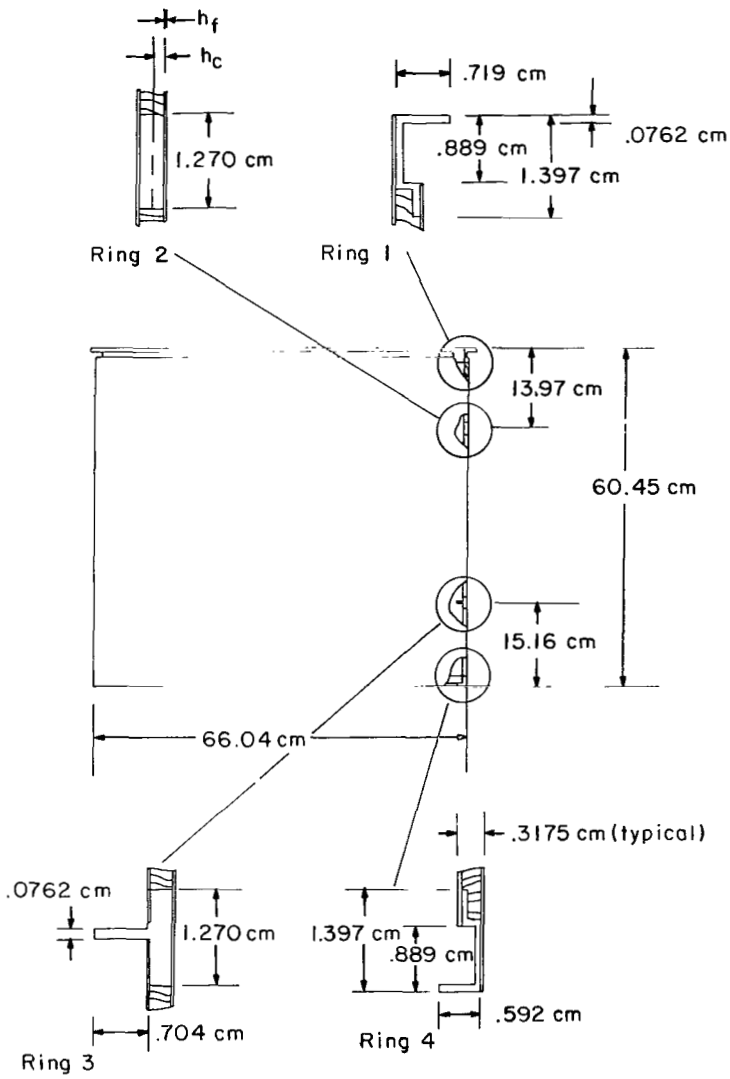

Figure 2.- Schematic drawing of cylinder 2.

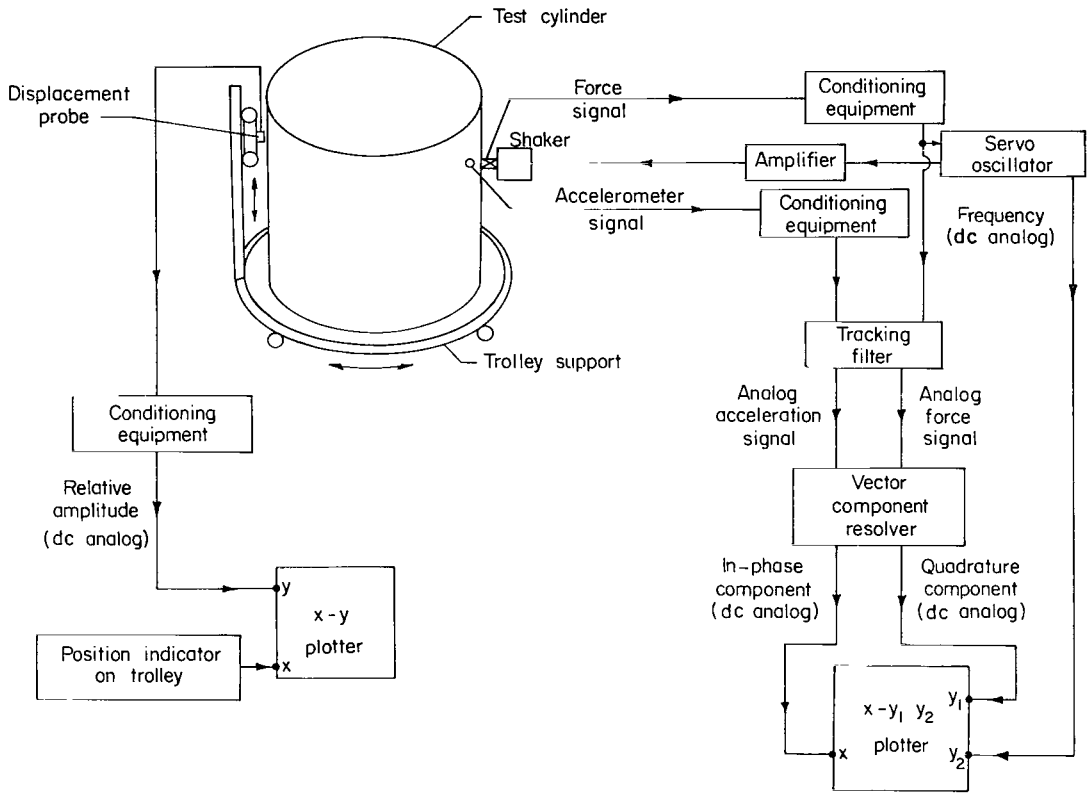

Figure 3.- Schematic view of instrumentation.

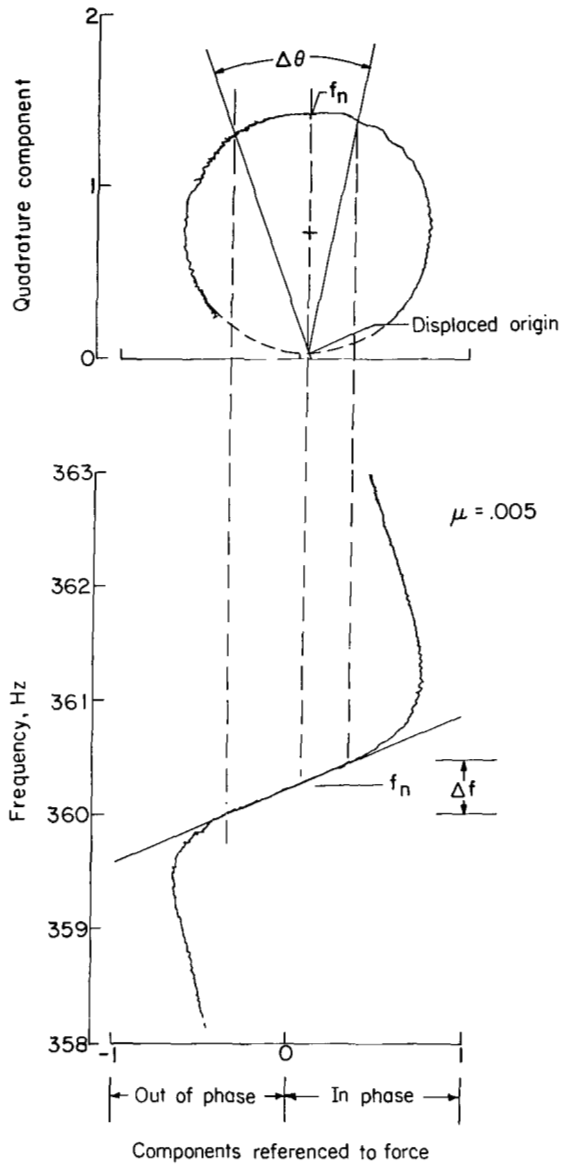

Figure 4.- Kennedy-Pancu plot of acceleration at the input-force location. Cylinder 2 with unrestrained edges; second lowest mode (mode 2) at n = 6.

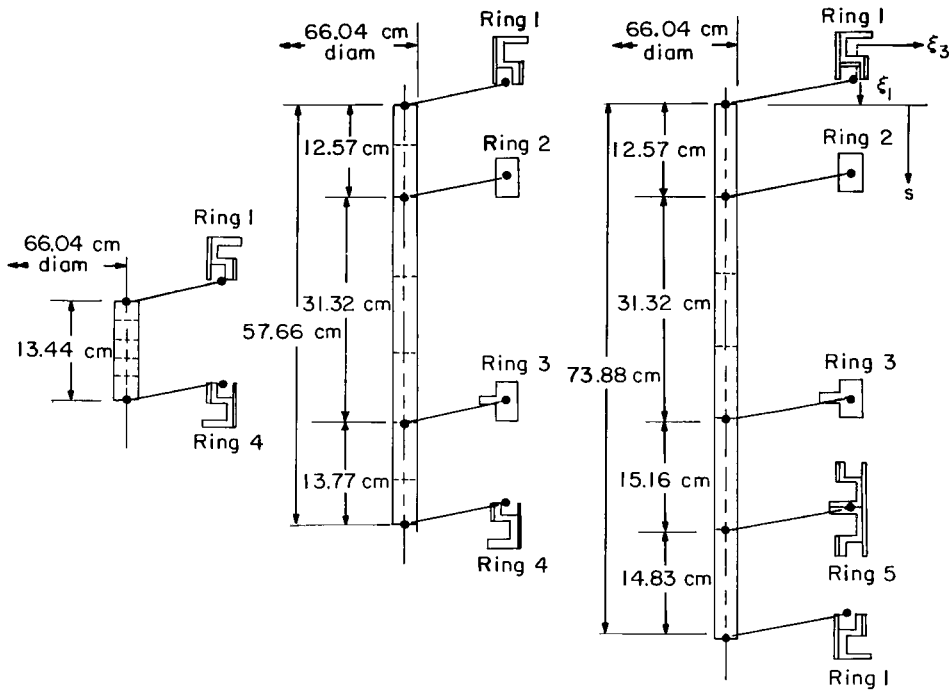

(a) Cylinder 1. (b) Cylinder 2. (c) Cylinder 3.

Figure 5.- Analytical representation of the shells and ring attachments.

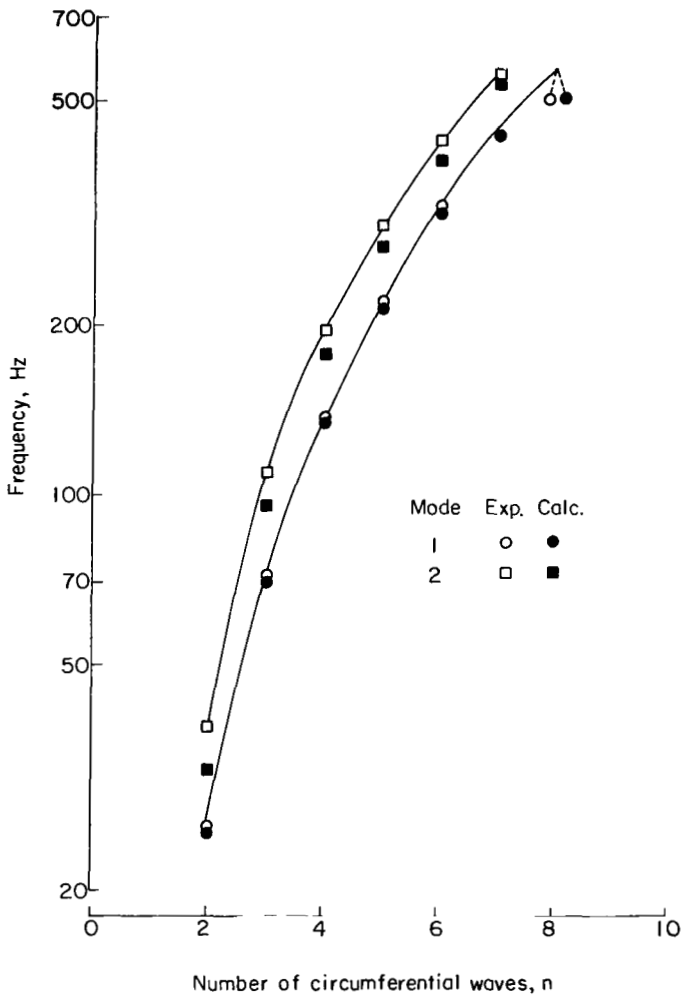

Figure 6.- Experimental and calculated frequencies as functions of number of circumferential waves for cylinder 1 with unrestrained edges.

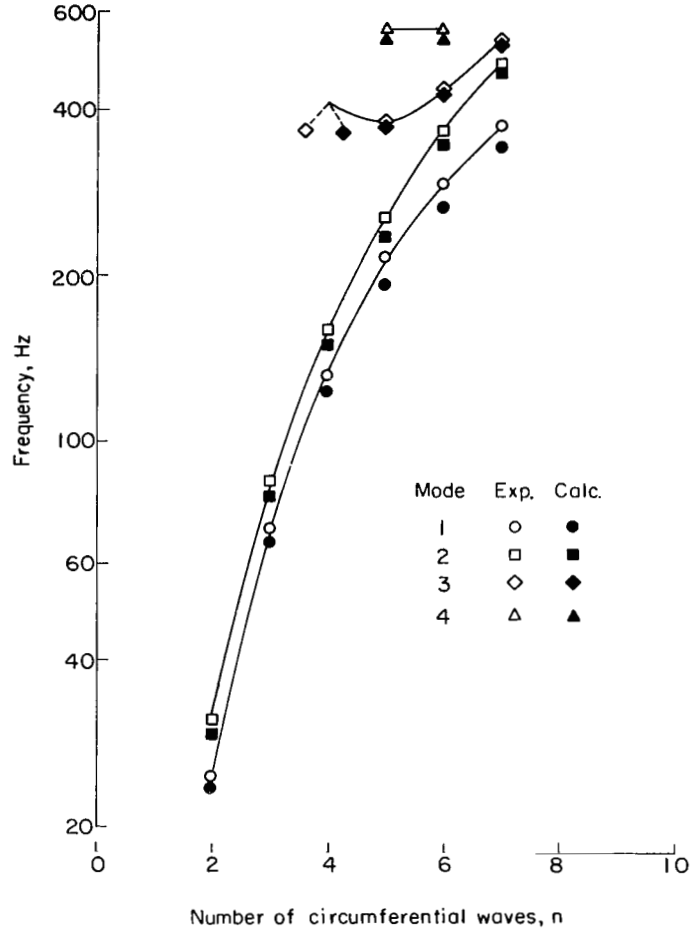

Figure 7.- Experimental and calculated frequencies as functions of number of circumferential waves for cylinder 2 with unrestrained edges.

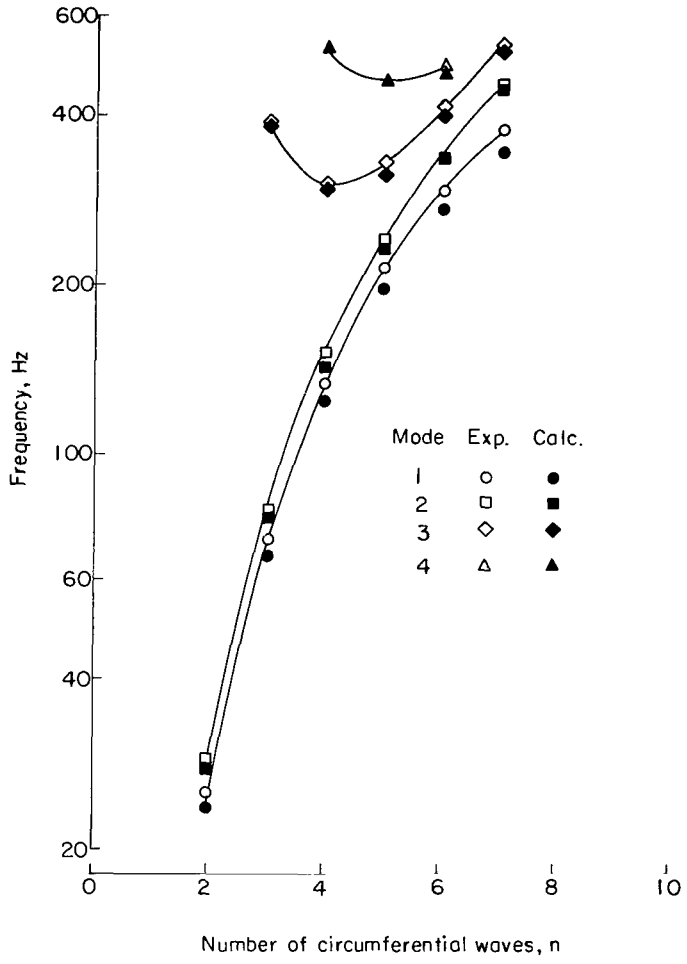

Figure 8.- Experimental and calculated frequencies as functions of number of circumferential waves for cylinder 3 with unrestrained edges.

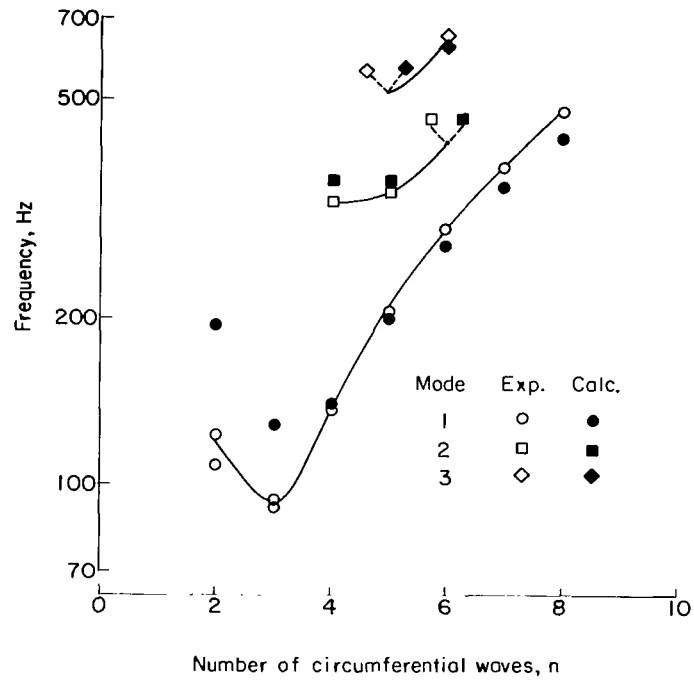

Figure 9.- Experimental and calculated frequencies as functions of number of circumferential waves for cylinder 2 with standard fasteners.

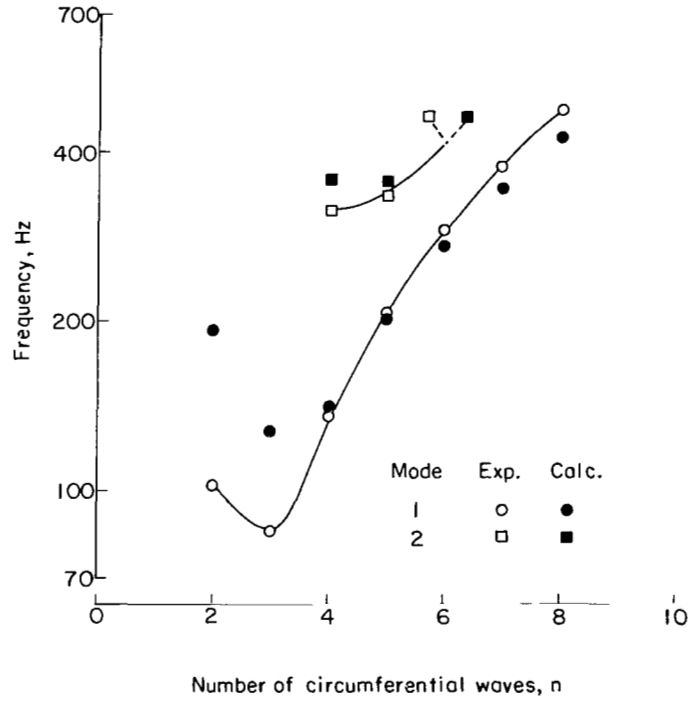

Figure 10.- Experimental and calculated frequencies as functions of number of circumferential waves for cylinder 2 with hinged joints.

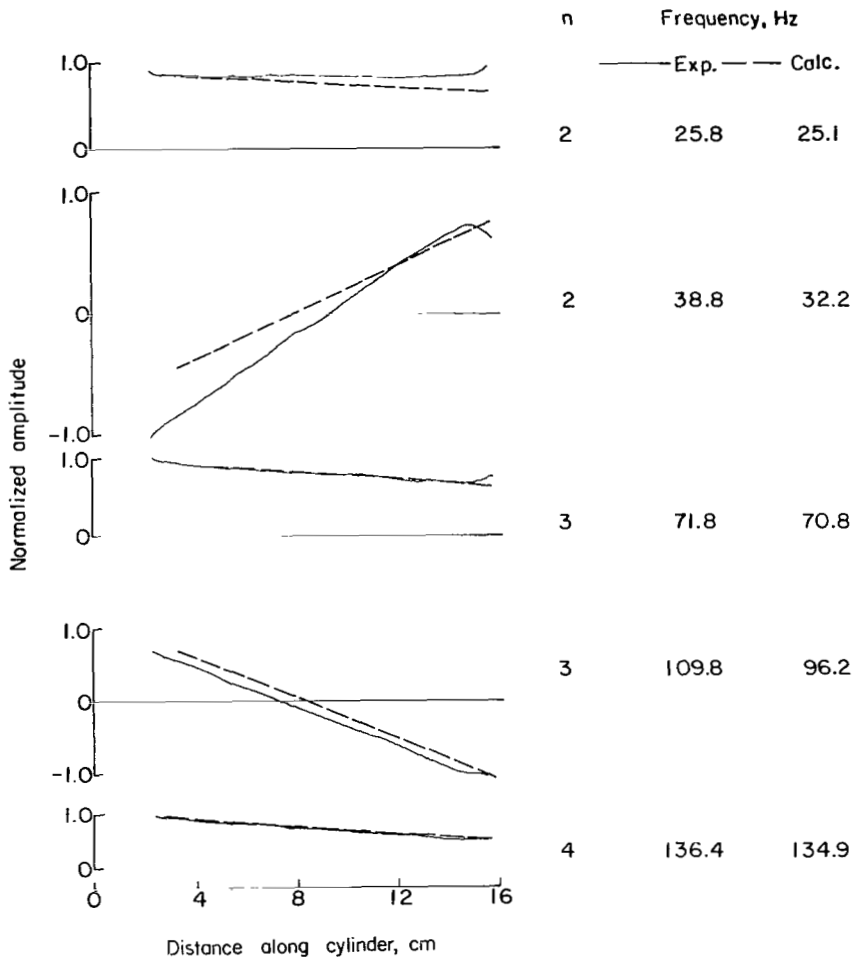

Figure 11.- Experimental resonant response shapes and calculated mode shapes for cylinder 1 with unrestrained edges.

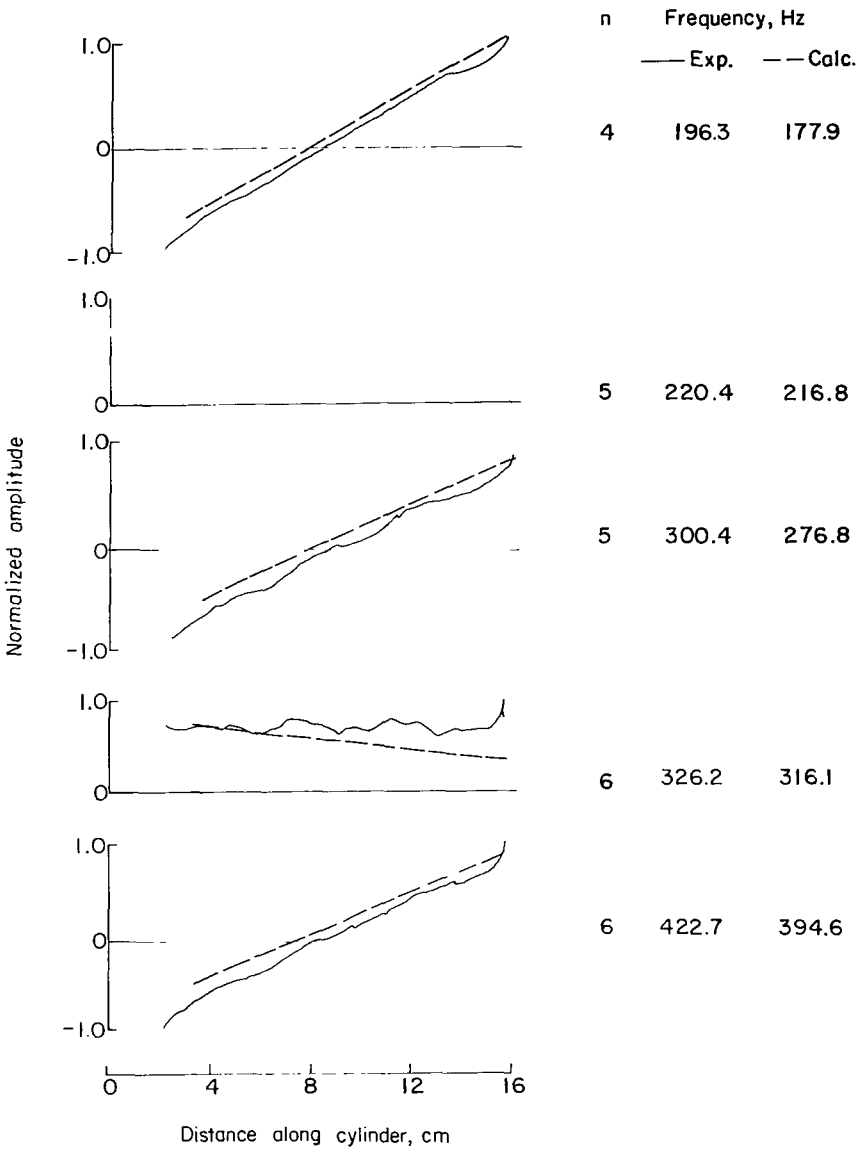

Figure 11.- Continued.

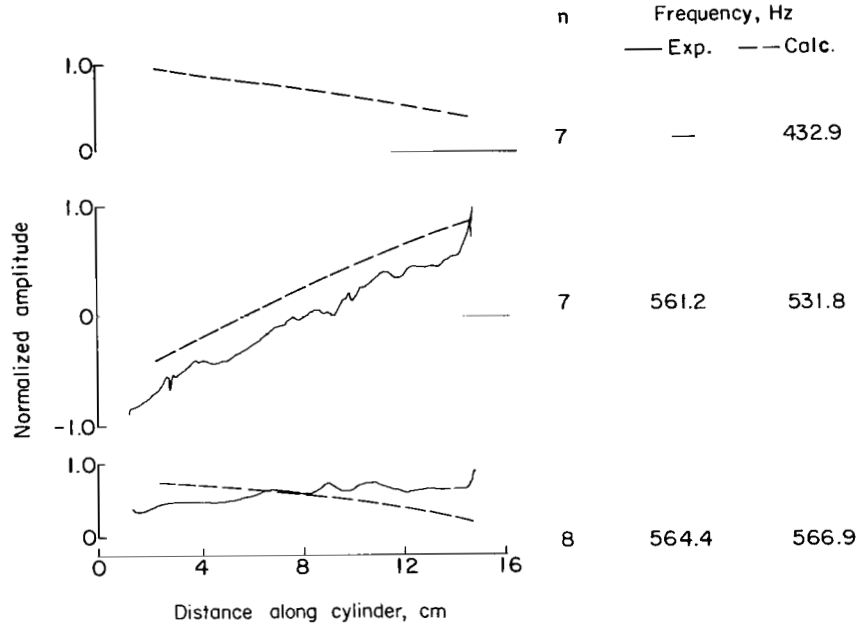

Figure 11.- Concluded.

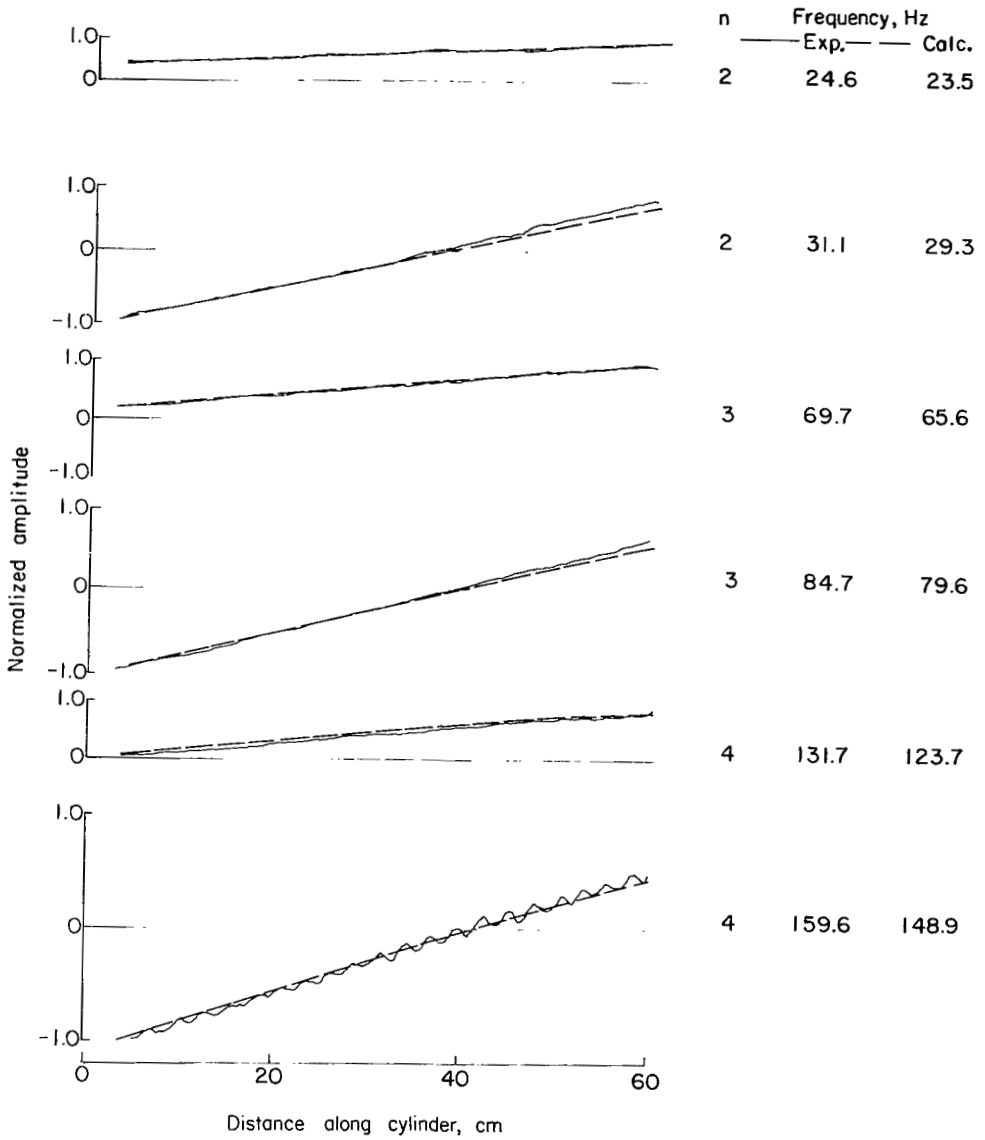

Figure 12.- Experimental resonant response shapes and calculated mode shapes for cylinder 2 with unrestrained edges.

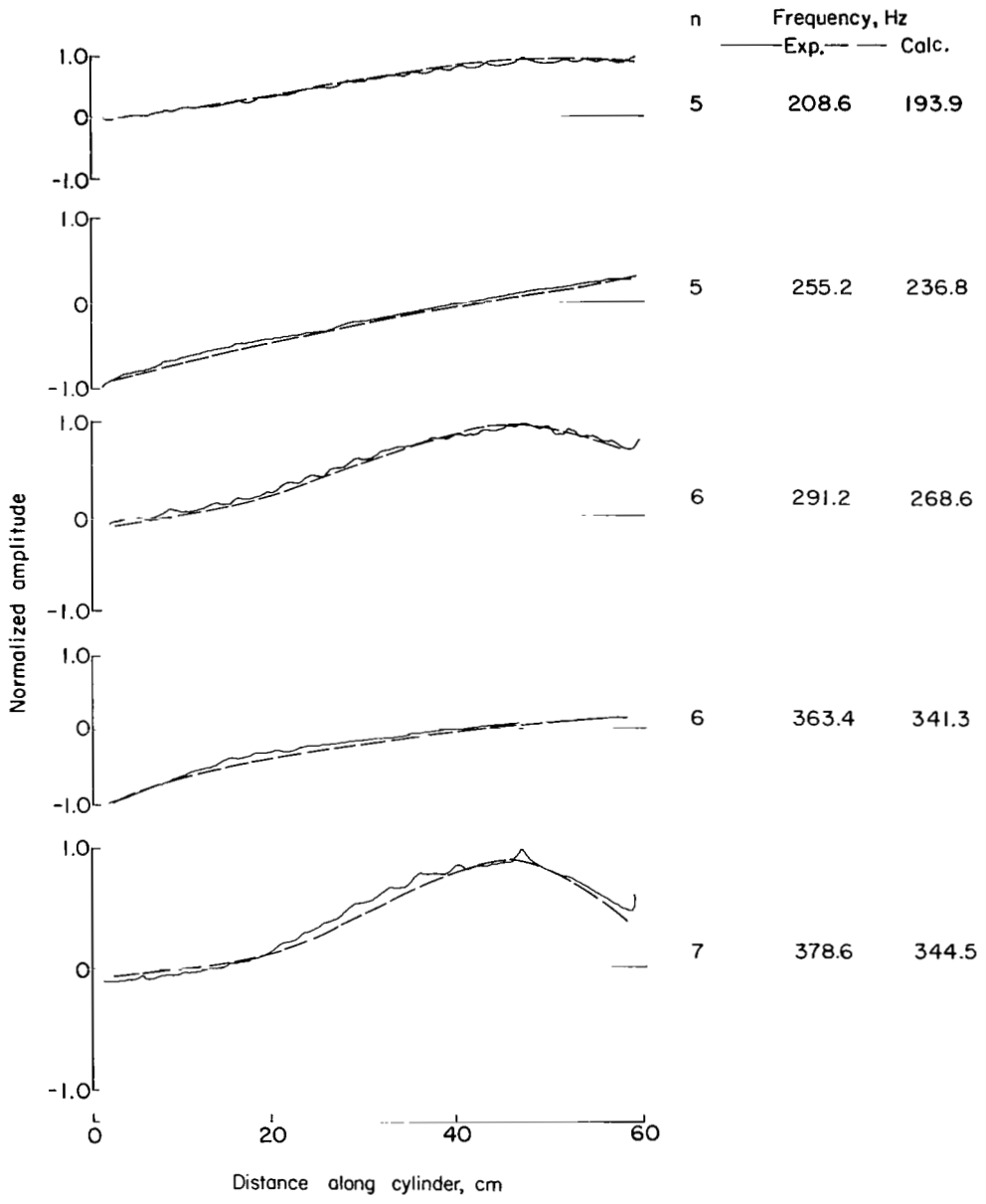

Figure 12.- Continued.

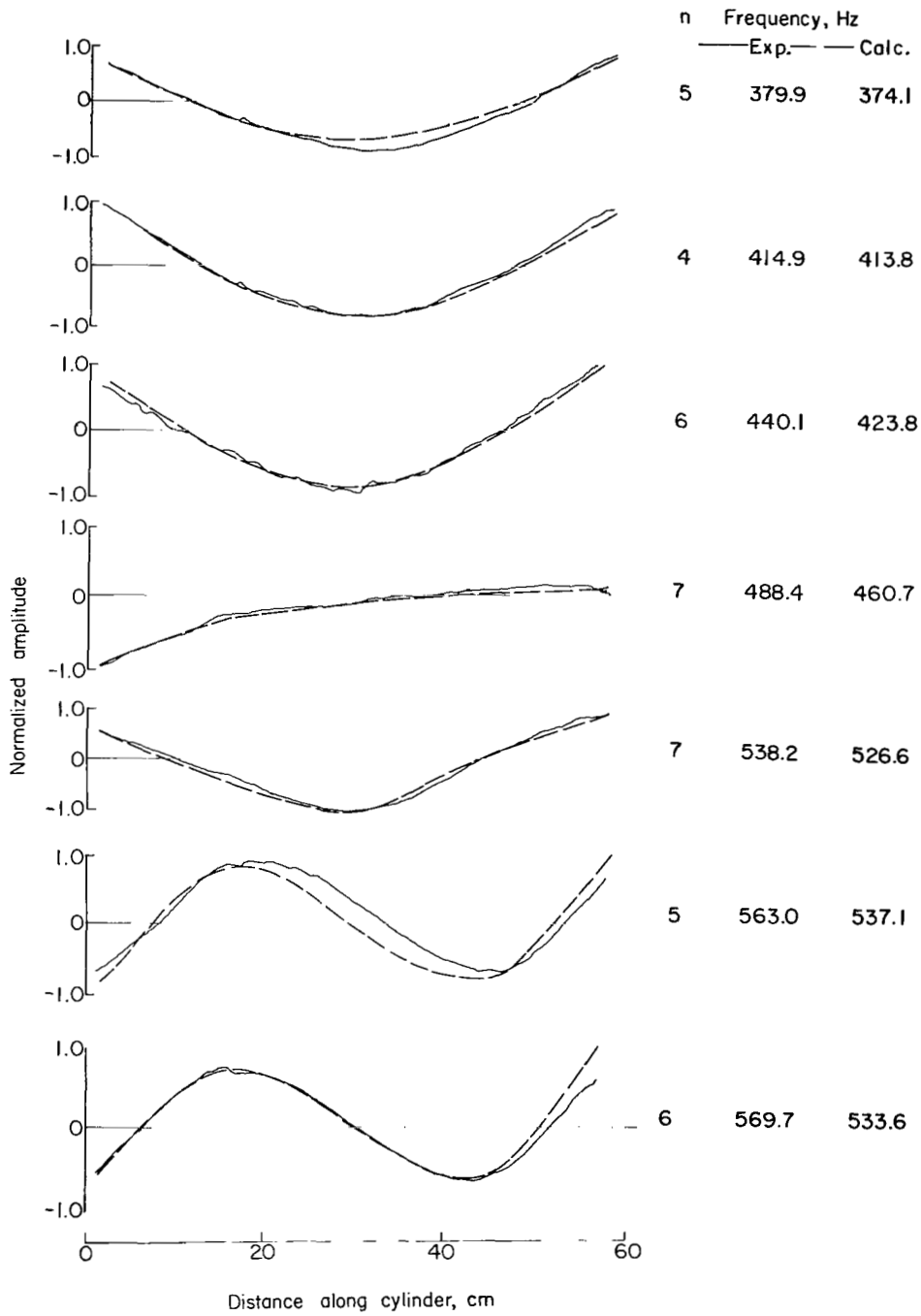

Figure 12.- Concluded.

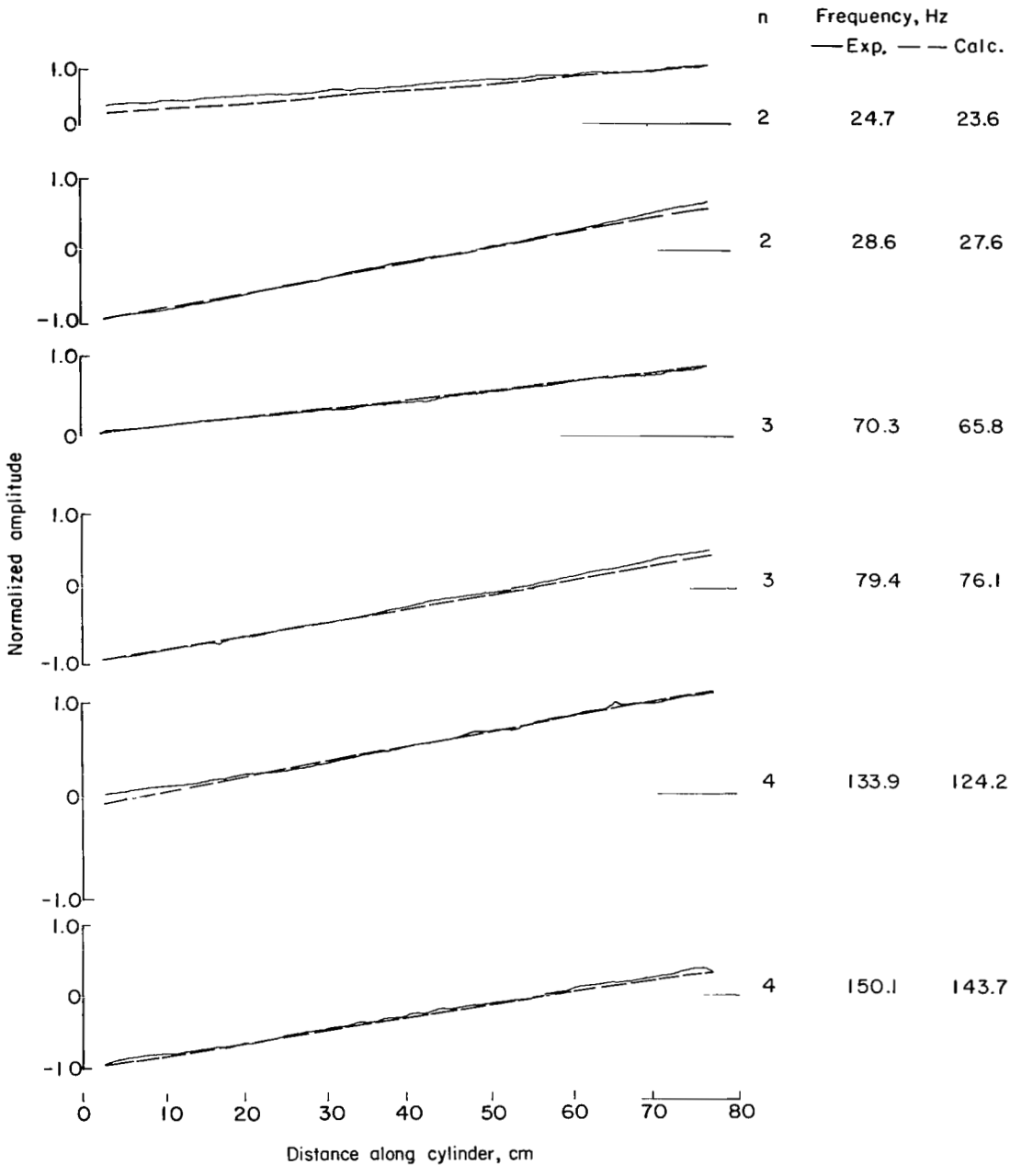

Figure 13.- Experimental resonant response shapes and calculated mode shapes for cylinder 3 with unrestrained edges. (The distance along the cylinder is measured from the top of the ring 1 that is attached at juncture 1.)

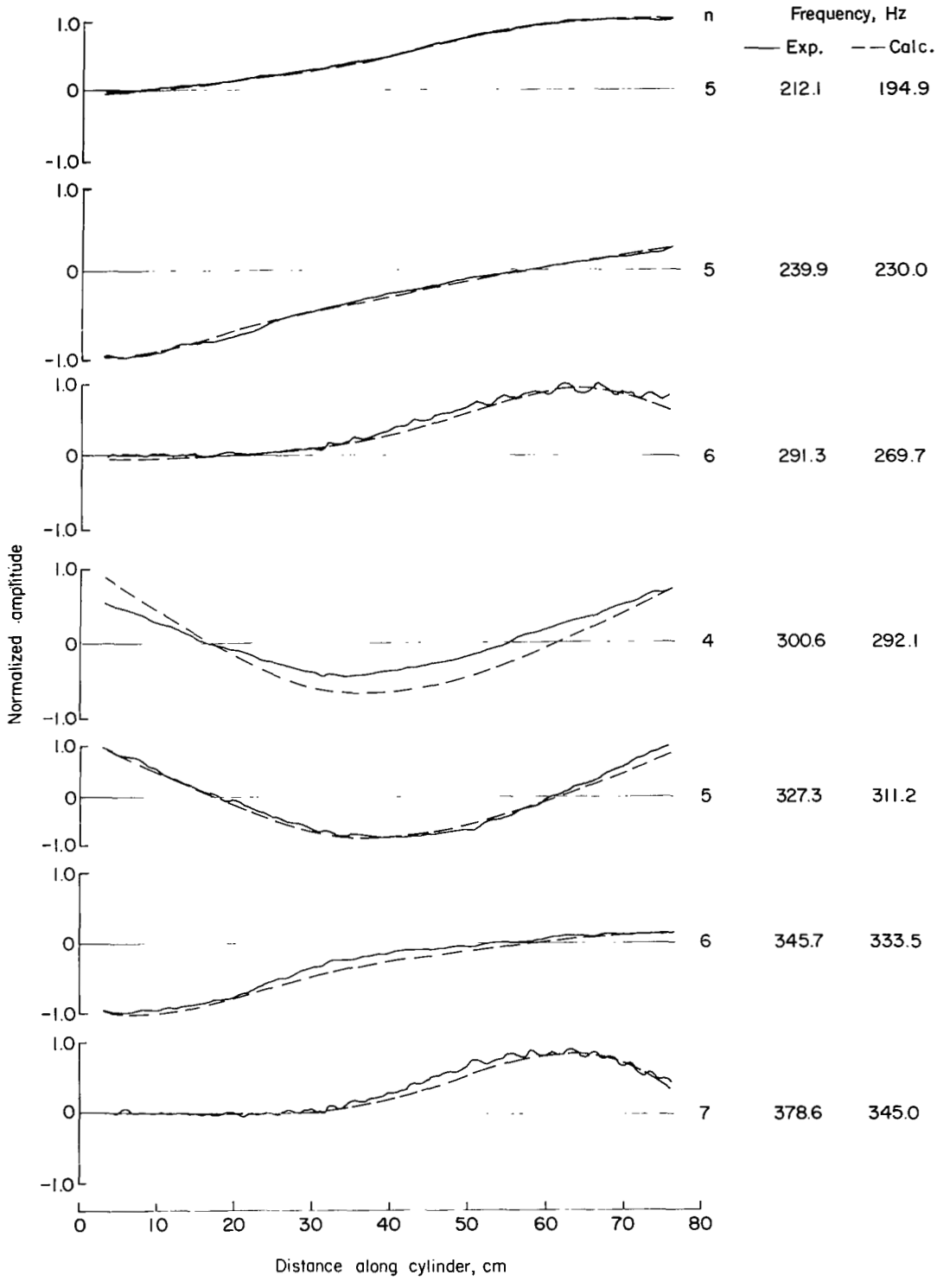

Figure 13.- Continued.

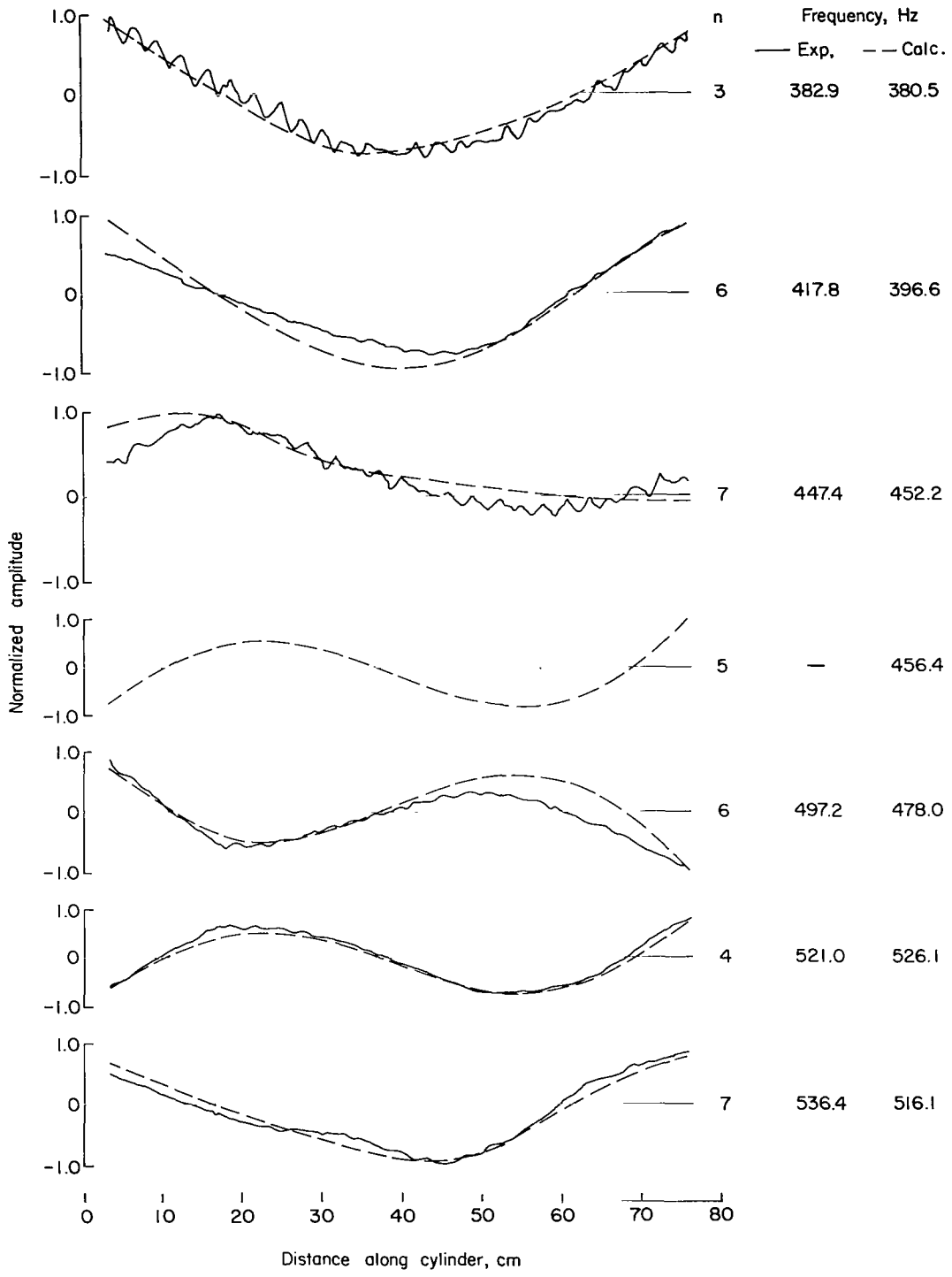

Figure 13.- Concluded.

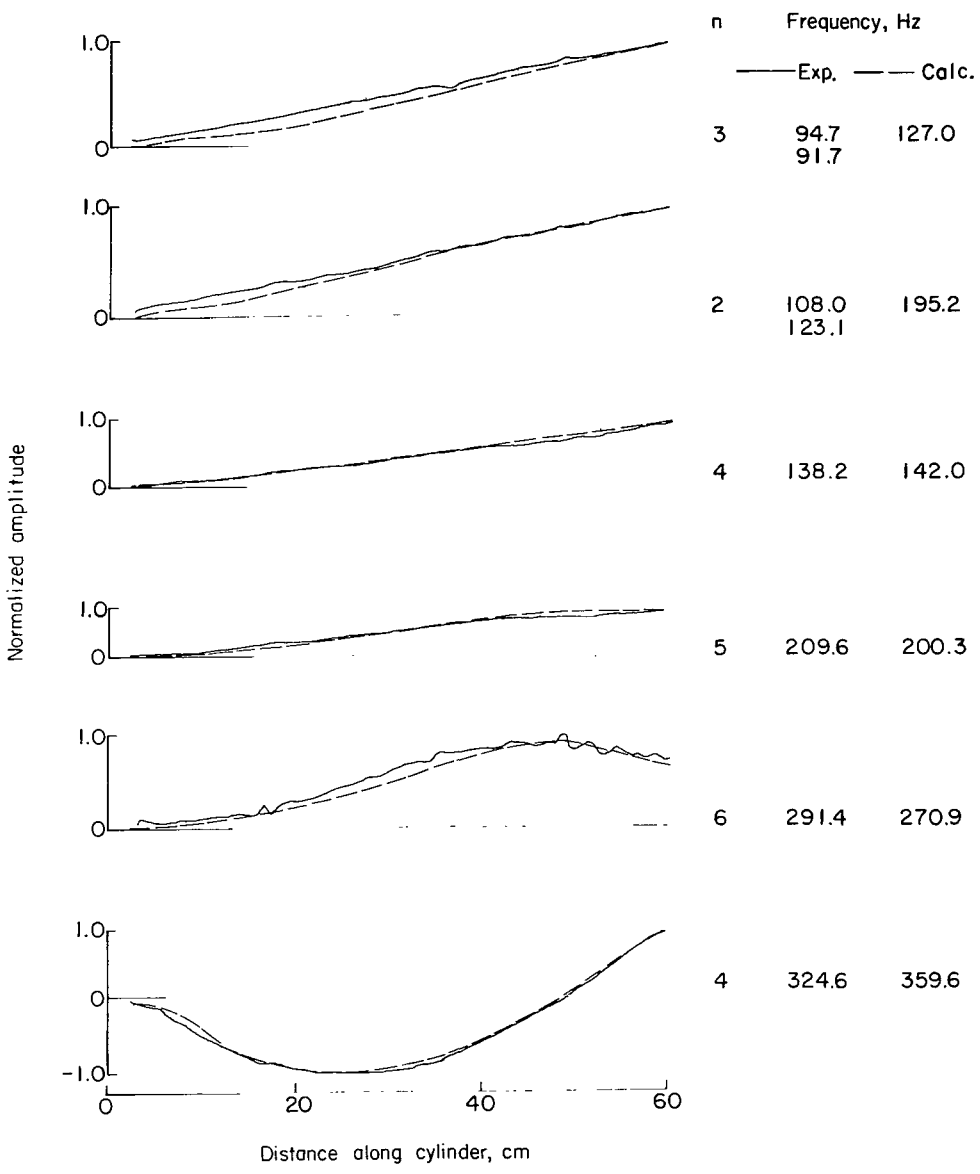

Figure 14.- Experimental resonant response shapes and calculated mode shapes for cylinder 2 with standard fasteners (clamped edges).

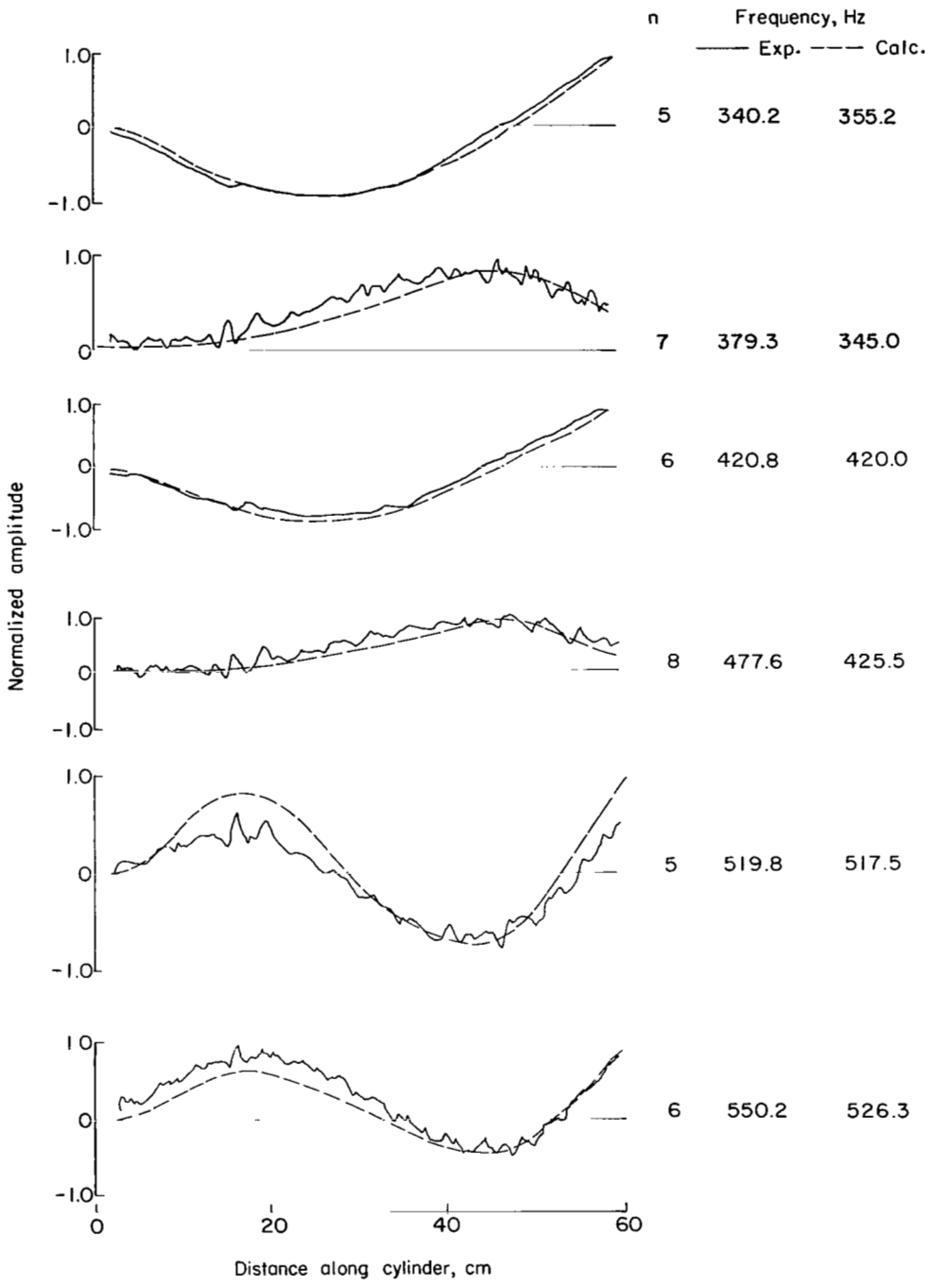

Figure 14.- Concluded.

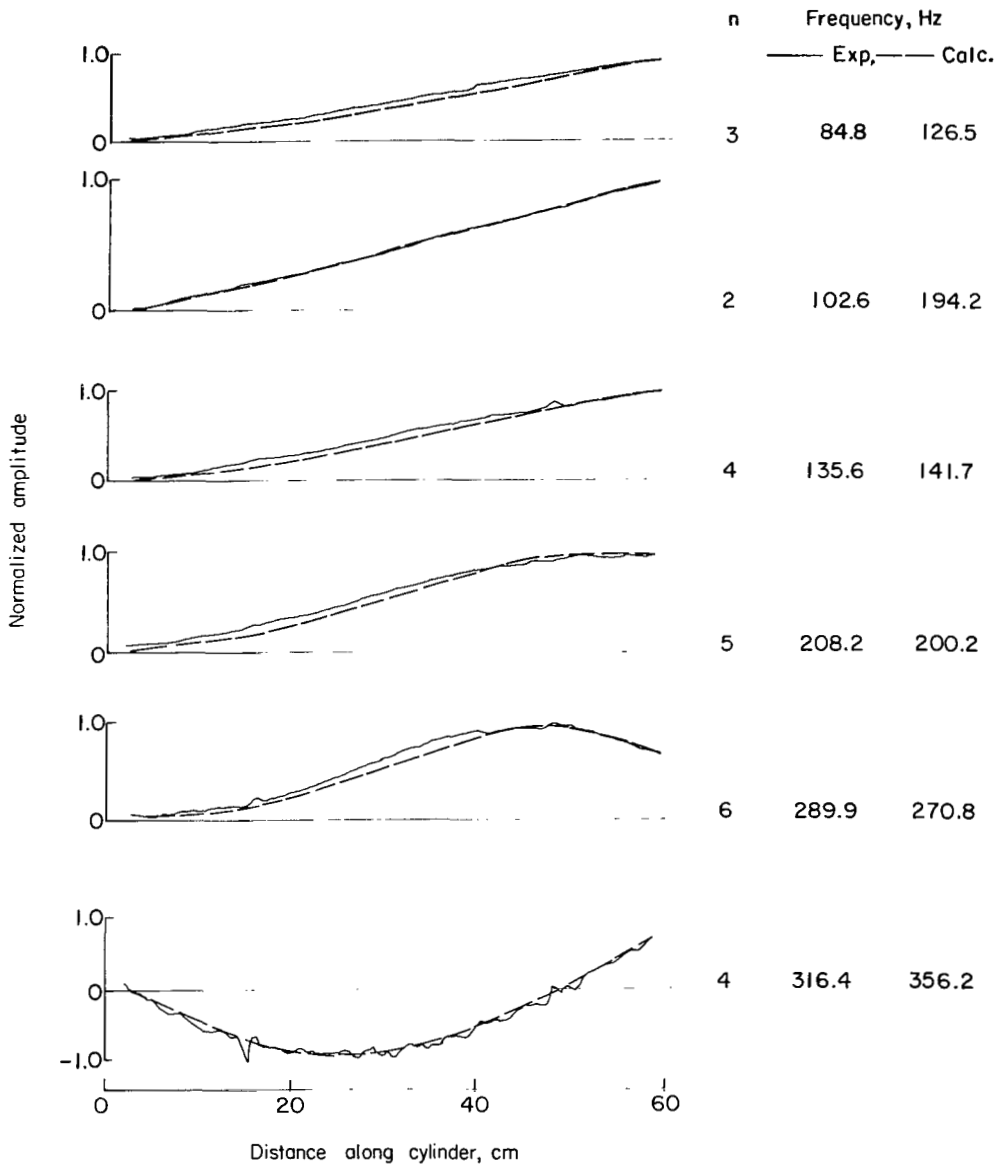

Figure 15.- Experimental resonant response shapes and calculated mode shapes for cylinder 2 with hinged joints (simply supported edges).

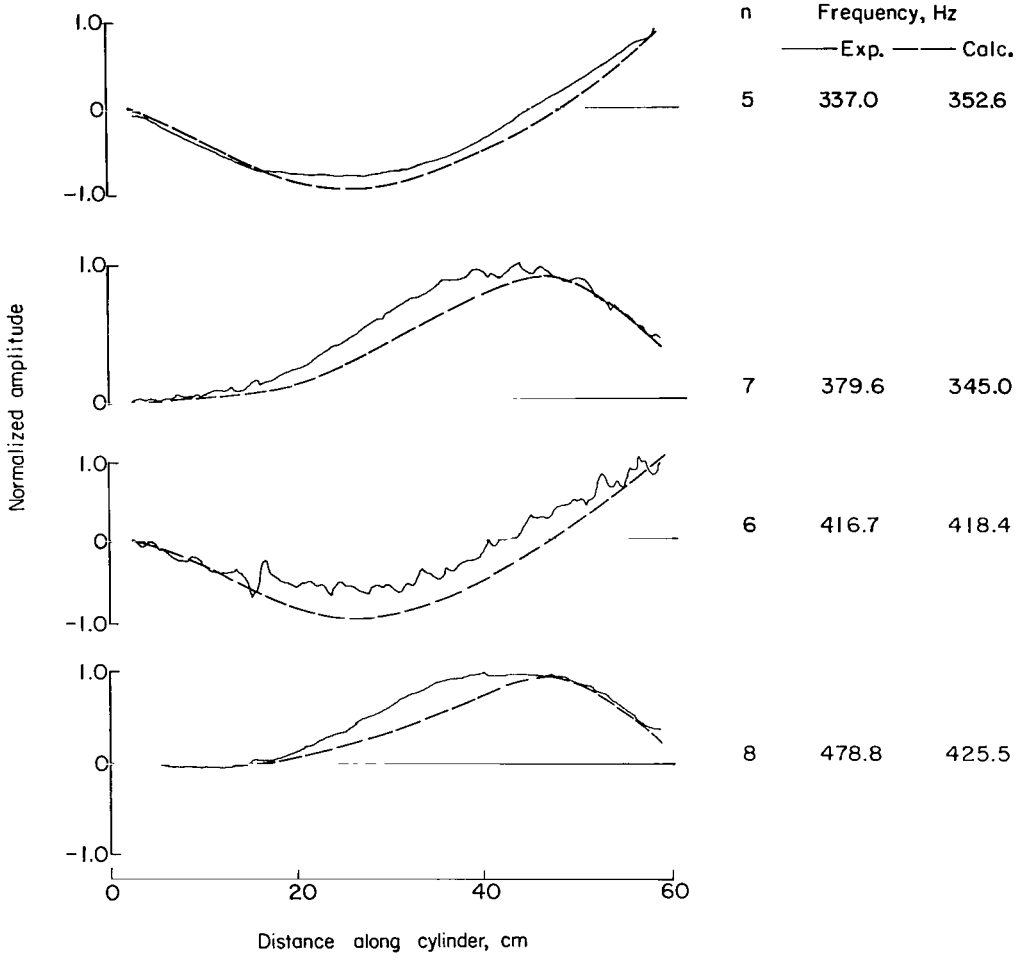

Figure 15.- Concluded.

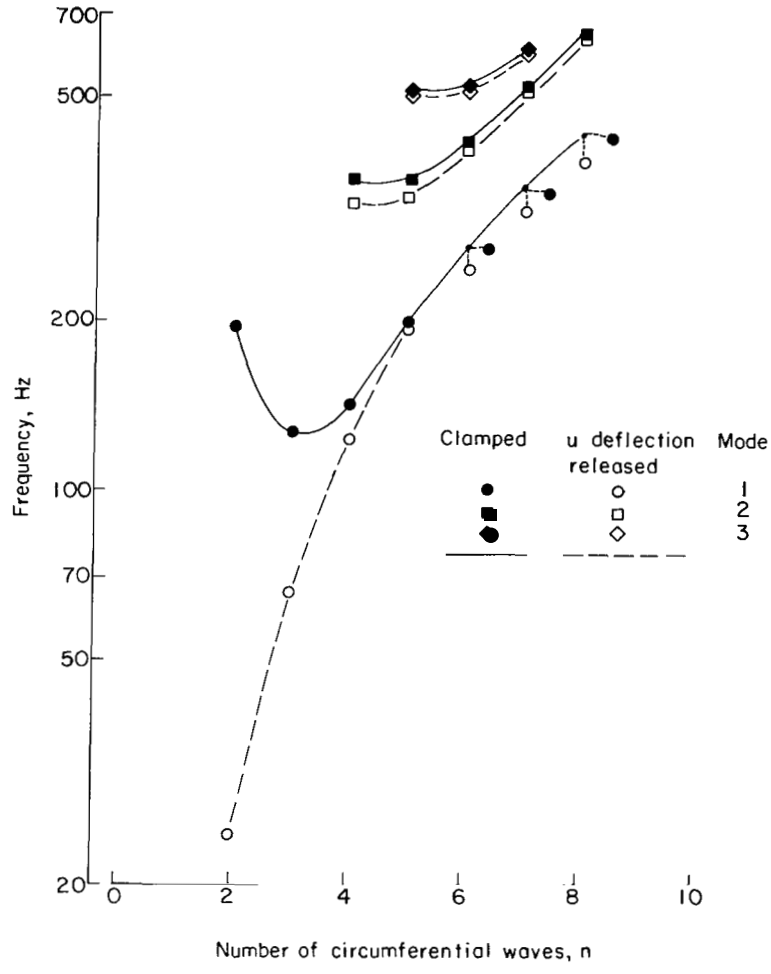

Figure 16.- Comparison of calculated frequencies as functions of number of circumferential waves for cylinder 2 with a clamped edge and cylinder 2 with the u deflection released.

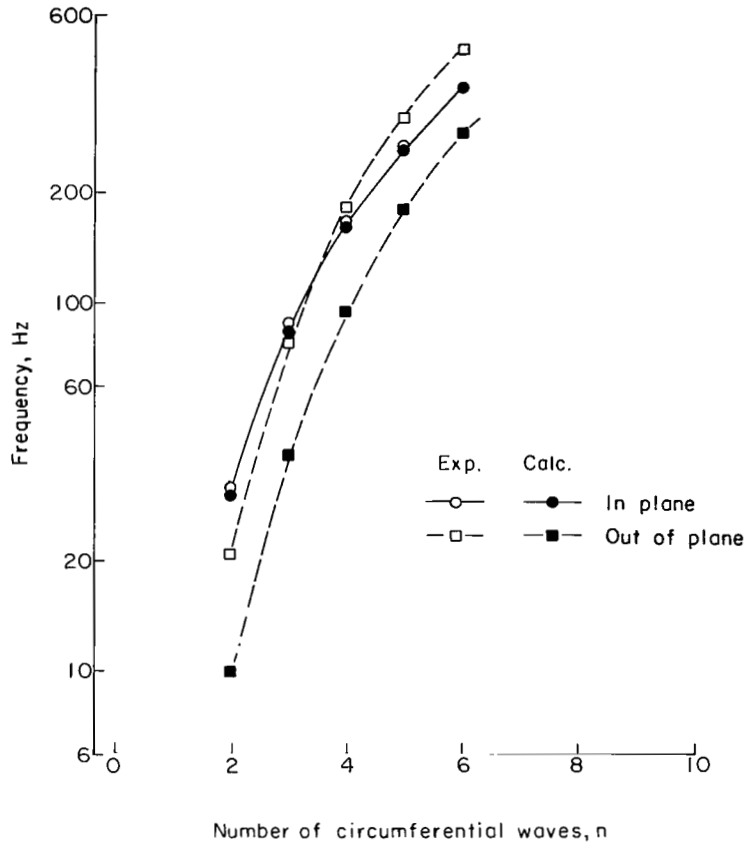

(a) Ring 1.

Figure 17.- Experimental and calculated frequencies as functions of number of circumferential waves n for rings 1 and 4 with clips.

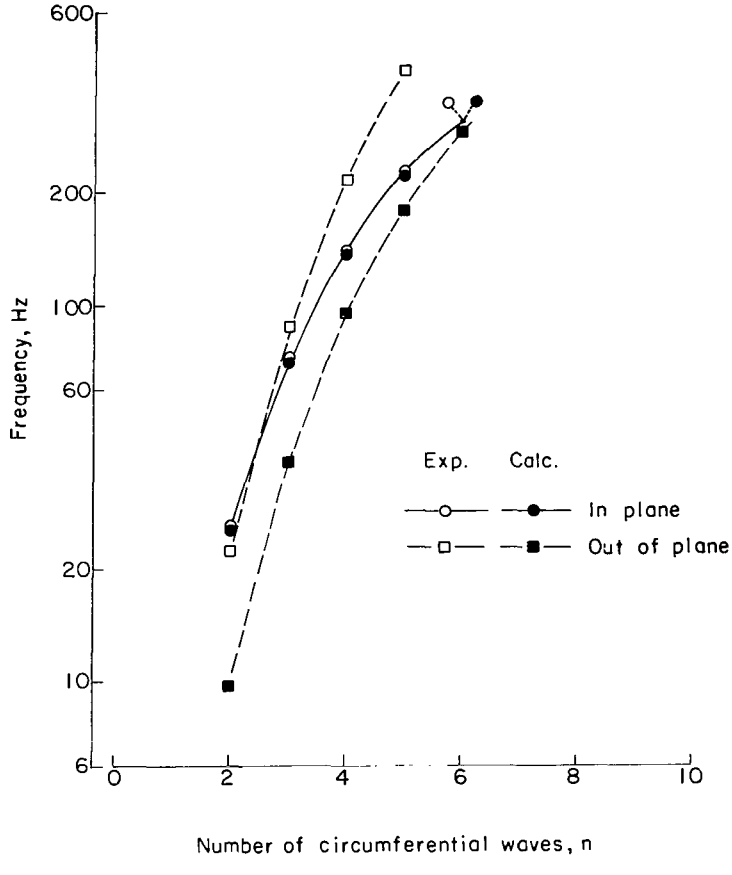

(b) Ring 4.

Figure 17.- Concluded.

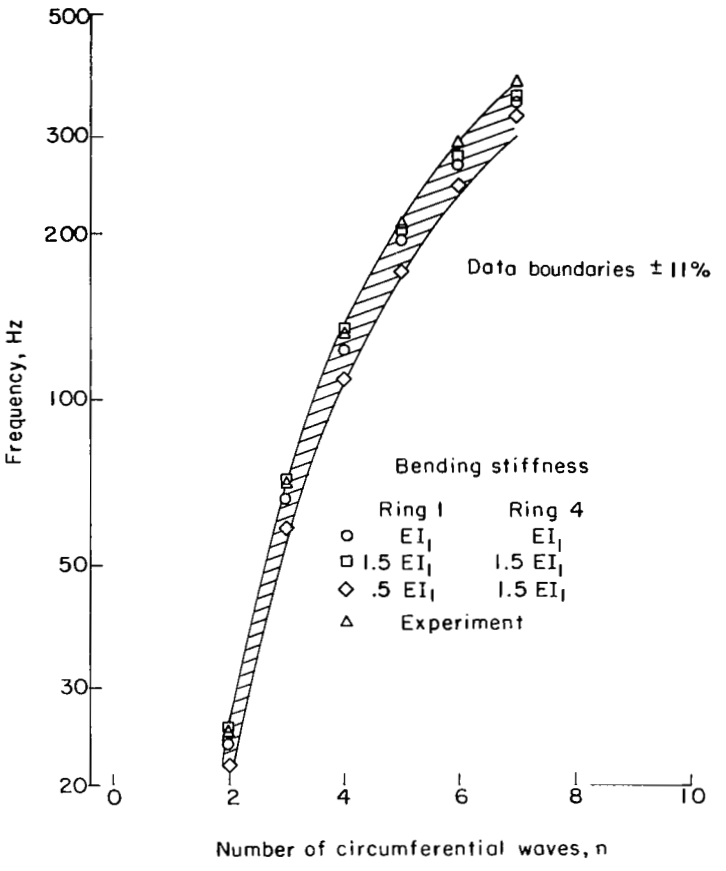

(a) Lowest frequency mode for any value of n.

Figure 18.- Comparison of experimental resonant frequencies with natural frequencies calculated by using modified values of EI_1. Cylinder 2 with unrestrained edges.

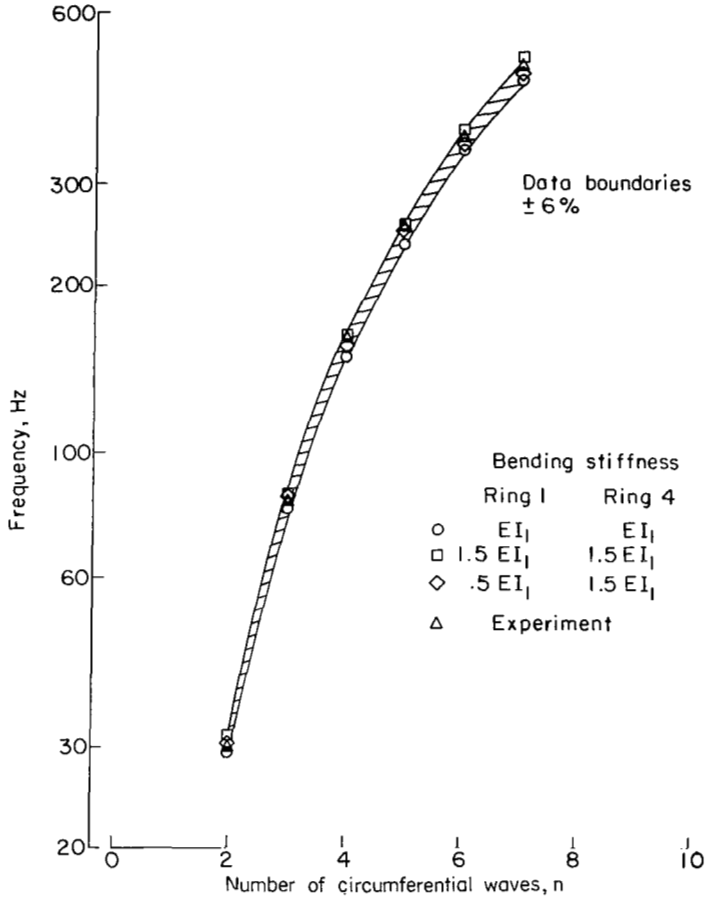

(b) Second lowest frequency mode for any value n.

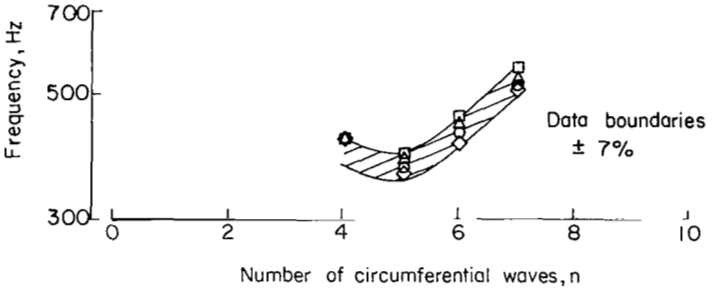

(c) Third lowest frequency mode for any value n.

Figure 18.- Concluded.

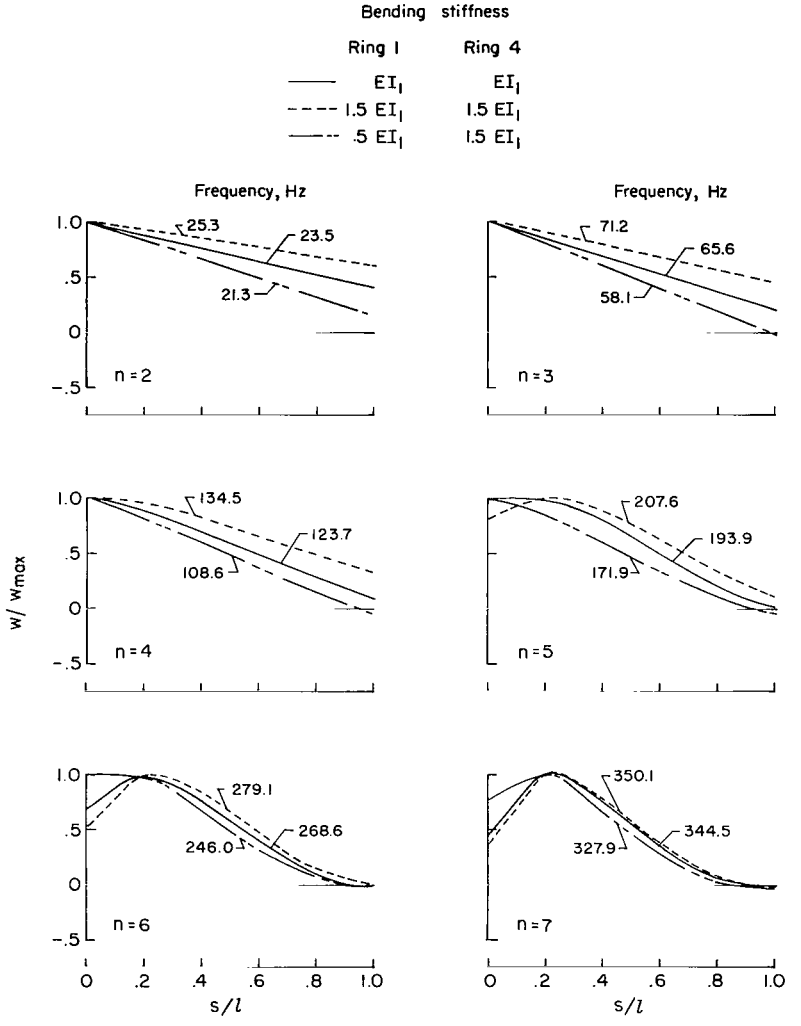

(a) Lowest frequency modes.

Figure 19.- Calculated mode shapes for modified values of EI_1 for rings 1 and 4. Cylinder 2 with unrestrained edges.

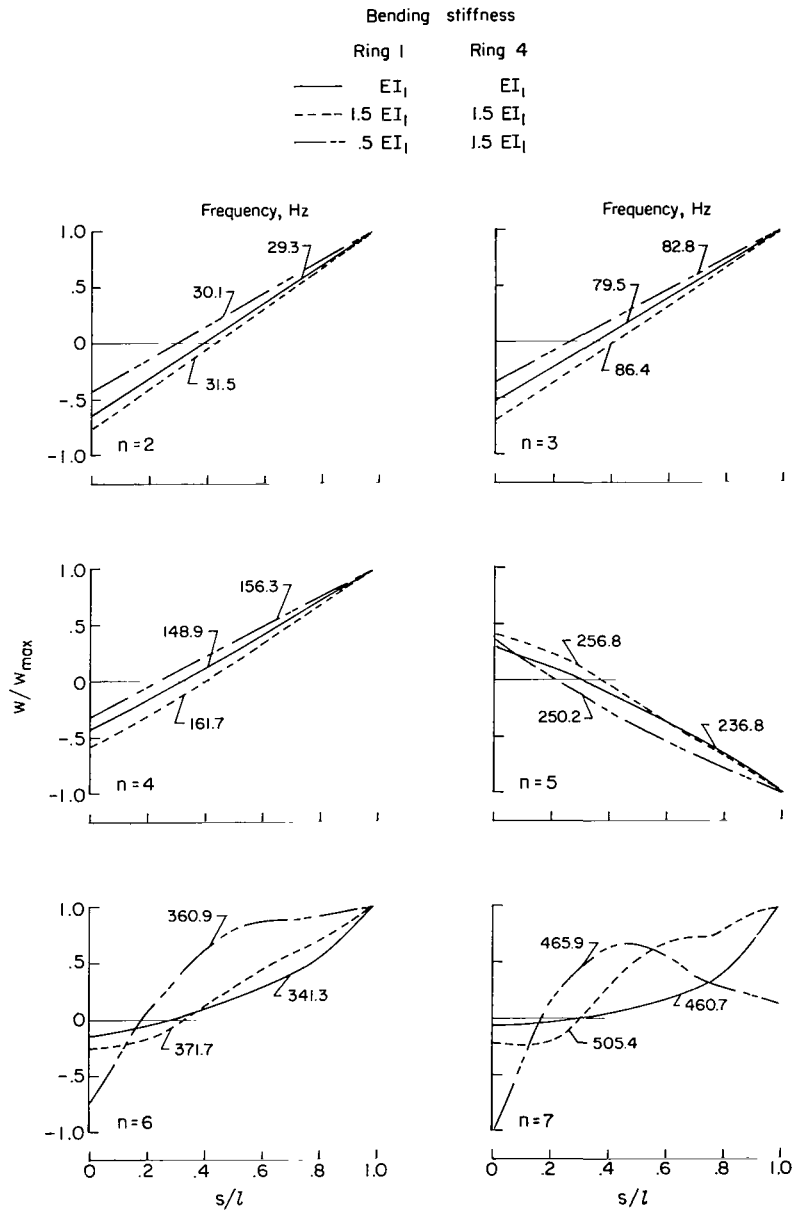

(b) Second lowest frequency modes.

Figure 19.- Continued.

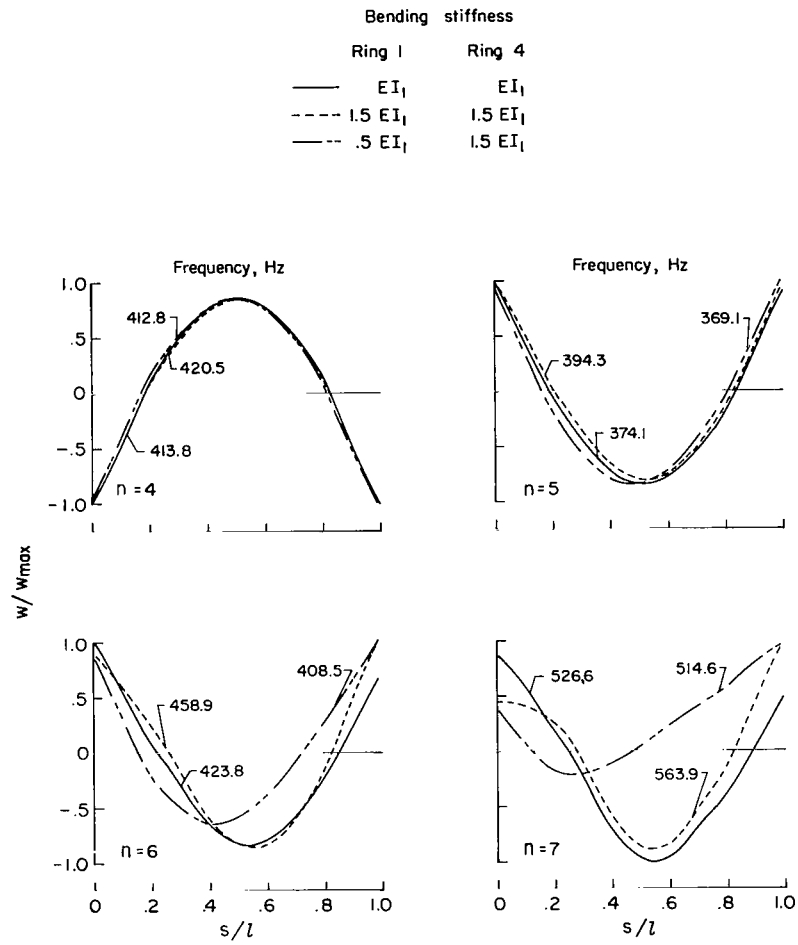

(c) Third lowest frequency modes.

Figure 19.- Concluded.

"The aeronautical and space activities of the United States shall be conducted so as to contribute . . . to the expansion of human knowledge of phenomena in the atmosphere and space. The Administration shall provide for the widest practicable and appropriate dissemination of information concerning its activities and the results thereof."

— NATIONAL AERONAUTICS AND SPACE ACT OF 1958

NASA SCIENTIFIC AND TECHNICAL PUBLICATIONS

TECHNICAL REPORTS: Scientific and technical information considered important, complete, and a lasting contribution to existing knowledge.

TECHNICAL NOTES: Information less broad in scope but nevertheless of importance as a contribution to existing knowledge.

TECHNICAL MEMORANDUMS: Information receiving limited distribution because of preliminary data, security classification, or other reasons.

CONTRACTOR REPORTS: Scientific and technical information generated under a NASA contract or grant and considered an important contribution to existing knowledge.

TECHNICAL TRANSLATIONS: Information published in a foreign language considered to merit NASA distribution in English.

SPECIAL PUBLICATIONS: Information derived from or of value to NASA activities. Publications include conference proceedings, monographs, data compilations, handbooks, sourcebooks, and special bibliographies.

TECHNOLOGY UTILIZATION PUBLICATIONS: Information on technology used by NASA that may be of particular interest in commercial and other non-aerospace applications. Publications include Tech Briefs, Technology Utilization Reports and Technology Surveys.

Details on the availability of these publications may be obtained from:

SCIENTIFIC AND TECHNICAL INFORMATION OFFICE

NATIONAL AERONAUTICS AND SPACE ADMINISTRATION

Washington, D.C. 20546